Jo et al. Cell Communication and Signaling (2026) 24:540
https://doi.org/10.1186/s12964-026-03082-w

Cell Communication and Signaling

RESEARCH Open Access

Targeting astrocyte-mediated neurotoxicity induced by ALS/FTD-associated RNA binding proteins

Myungjin Jo[1,5†], Seyeon Kim[1†], Junghwa Woo[1], Jin-Sung Park[2,6], Seung Hyun Kim[3,4], Minyeop Nahm[1], Sang Ryong Kim[5,6], Shinrye Lee[1*] and Hyung-Jun Kim[1,7*]

Abstract

Background Amyotrophic lateral sclerosis (ALS) and frontotemporal dementia (FTD) are neurodegenerative disorders characterized by reactive astrocytes that contribute to neuronal injury through TAR DNA-binding protein 43 (TDP-43)-or fused in sarcoma (FUS)-driven neuroinflammatory signaling. Dehydrocostus lactone (DHE), a blood-brain barrier-permeable sesquiterpene lactone with established anti-inflammatory activity, represents a promising but unexplored therapeutic candidate for ALS/FTD.

Methods The therapeutic effects of DHE were evaluated in primary mouse and human astrocytes expressing ALS/FTD-associated RNA-binding protein pathology, ALS patient-derived fibroblasts, and primary cortical neurons exposed to astrocyte-conditioned medium. *Drosophila* models expressing mutant FUS or TDP-43 in glial cells were used to assess locomotor performance and survival. Molecular analyses examined nuclear factor kappa B (NF-κB) signaling, nuclear factor erythroid 2-related factor 2 (NRF2)-dependent antioxidant responses, protein aggregation, mitochondrial function, and inflammatory mediator production. Plasma concentrations of inflammatory cytokines and chemokines were measured in patients with sporadic ALS.

Results DHE exerted neuroprotective effects through a dual mechanism involving suppression of NF-κB-dependent inflammatory signaling and activation of NRF2-mediated antioxidant pathways in astrocytes exhibiting FUS or TDP-43 proteinopathy. DHE attenuated astrocyte-mediated neurotoxicity and improved neuronal mitochondrial function in conditioned-medium assays. In addition, DHE reduced pathological FUS accumulation in FUS P525L-expressing astrocytes and in stress-challenged patient-derived fibroblasts. In *Drosophila* models, DHE significantly improved locomotor function and extended survival. Translationally, the chemokines CXCL10, CCL3, and CCL19 were elevated in plasma from patients with ALS, were induced by FUS or TDP-43 pathology in astrocytes, and were suppressed by DHE treatment, supporting the clinical relevance of the inflammatory pathways targeted by DHE.

†Myungjin Jo and Seyeon Kim contributed equally to this work.

*Correspondence:
Shinrye Lee
srlee@kbri.re.kr
Hyung-Jun Kim
kijang1@kbri.re.kr; kijang1@gmail.com

Full list of author information is available at the end of the article

© The Author(s) 2026. **Open Access** This article is licensed under a Creative Commons Attribution-NonCommercial-NoDerivatives 4.0 International License, which permits any non-commercial use, sharing, distribution and reproduction in any medium or format, as long as you give appropriate credit to the original author(s) and the source, provide a link to the Creative Commons licence, and indicate if you modified the licensed material. You do not have permission under this licence to share adapted material derived from this article or parts of it. The images or other third party material in this article are included in the article's Creative Commons licence, unless indicated otherwise in a credit line to the material. If material is not included in the article's Creative Commons licence and your intended use is not permitted by statutory regulation or exceeds the permitted use, you will need to obtain permission directly from the copyright holder. To view a copy of this licence, visit http://creativecommons.org/licenses/by-nc-nd/4.0/.

Conclusion DHE mitigates astrocyte-driven neurotoxicity associated with ALS/FTD-related RNA-binding protein pathology by suppressing inflammatory signaling and enhancing antioxidant defense mechanisms. The consistent therapeutic effects observed across mouse and human cellular models, patient-derived samples, and *in vivo Drosophila* models support further investigation of DHE as a potential therapeutic strategy for ALS/FTD and highlight astrocyte-mediated signaling pathways as actionable targets in neurodegenerative disease.

Keywords Amyotrophic lateral sclerosis, Frontotemporal dementia, Astrocytes, Neuroinflammation, Oxidative stress, Mitochondrial dysfunction, RNA-binding proteins, Chemokines

Background

Dehydrocostus lactone (DHE), a sesquiterpene lactone isolated from medicinal plants, has attracted considerable interest because of its anti-inflammatory, antioxidant, and anticancer activities [1–6]. DHE can cross the blood–brain barrier (BBB) and exert biological effects within the central nervous system (CNS); however, its therapeutic potential in neurodegenerative diseases and its impact on neuroinflammatory processes remain largely unexplored [7]. Oral administration of DHE reportedly produces antidepressant-like effects in murine models, including the forced swim and tail suspension tests, although the underlying mechanisms within the CNS have not been fully elucidated [8].

Astrocytes are among the most abundant cell types in the CNS and play essential roles in maintaining neuronal homeostasis, regulating synaptic activity, and supporting metabolic and antioxidant functions. Increasing evidence implicates astrocyte dysfunction in the pathogenesis of amyotrophic lateral sclerosis (ALS) and frontotemporal dementia (FTD), two neurodegenerative disorders that constitute a disease spectrum with overlapping clinical, genetic, and pathological features [9]. During disease progression, astrocytes undergo reactive transformation and shift from neuroprotective to pro-inflammatory and neurotoxic states, thereby contributing to neuronal dysfunction and degeneration [9, 10]. Reactive astrocytes promote neurodegeneration through both loss-of-function and gain-of-toxic function mechanisms, including impaired glutamate clearance, metabolic dysregulation, disrupted calcium homeostasis, mitochondrial dysfunction, and the release of inflammatory mediators, and pathogenic extracellular vesicles [9–13]. These observations highlight astrocytes as key drivers of disease progression and attractive therapeutic targets in ALS and FTD.

Mislocalization and aggregation of RNA-binding proteins, particularly TAR DNA-binding protein 43 (TDP-43) and Fused in Sarcoma (FUS), are defining pathological features of ALS and FTD [14, 15]. Although disease-related mechanisms have been studied primarily in neurons, accumulating evidence indicates that astrocytes actively contribute to pathogenesis. TDP-43 and FUS proteinopathy disrupt astrocyte function through nuclear depletion of these RNA-binding proteins, cytoplasmic aggregation, and induction of pro-inflammatory signaling pathways that promote neurotoxicity. TDP-43 pathology noted in the vast majority of ALS cases and in a substantial proportion of FTD cases, impairs RNA metabolism, alters astrocyte morphology, and drives the acquisition of neurotoxic reactive phenotypes [11, 16–18]. Likewise, pathogenic FUS mutations induce astrocyte reactivity, enhance susceptibility to inflammatory stimuli, and stimulate the release of pro-inflammatory mediators, including tumor necrosis factor-α (TNF-α), thereby contributing to excitotoxicity and motor neuron degeneration [19–21].

Given the central role of astrocyte-mediated neurotoxicity in ALS/FTD and the established anti-inflammatory properties of DHE, we investigated whether DHE could mitigate pathological astrocyte responses induced by TDP-43 and FUS proteinopathy. Using complementary cellular, patient-derived, and in vivo models, we evaluated the neuroprotective effects of DHE and examined the molecular pathways underlying its activity. Our findings identify DHE as a modulator of astrocyte-associated pathogenic signaling and support its potential as a therapeutic as a therapeutic strategy for ALS/FTD.

Methods

Reagents

The following reagents were purchased from the indicated supplies: DHE (42575) [Sigma-Aldrich]; sodium arsenite ($NaAsO_2$, 106277) and Ethanol (EtOH, 1.00983.1011) [Merck-Millipore]; Recombinant human IL-1β protein (200-LB-010), Recombinant human TNF-α protein (210-TA-020), Recombinant human IFN-γ protein (285-IF-100) [R&D Systems].

Antibodies

The following antibodies were used for immunoblotting: rabbit anti-FUS (A300-292 A) [Bethyl Laboratories]; rabbit anti-FUS (NB100-561) [Novus Biologicals]; rabbit anti-TDP-43 (10782-2-AP) [Proteintech]; rabbit anti-phospho-IKKα/β (Ser176/180) (2697), rabbit anti-IKKβ (8943), mouse anti- phospho-IκBα (Ser32/36) (9246), rabbit anti-IκBα (4812), rabbit anti- phospho-NF-κB p65 (Ser536) (3033), rabbit anti-NF-κB (8242), mouse anti-HDAC1 (5356), HRP-conjugated anti-α-tubulin (9099), HRP-conjugated anti-rabbit IgG (7074), and

HRP-conjugated anti-mouse IgG (7076) [Cell Signaling Technology]; rabbit anti-β actin (ab16039) [abcam]; mouse-anti-β actin (TA811000) [OriGene Technologies].

Primary cell cultures

Primary cortical neuron cultures were prepared from embryonic day 16 (E16) C57BL/6 mouse embryos as described [22, 23]. Briefly, embryos were decapitated, and the brains were rapidly isolated and transferred to Hank's Balanced Salt Solution (HBSS; Gibco™, Thermo Fisher Scientific). Cerebral cortices were dissected, washed twice with HBSS, and enzymatically dissociated with papain (20 U/mL; Worthington Biochemical Corporation) and DNase I (0.005%) for 30 min at 37 °C. The tissue was mechanically dissociated by gentle trituration using 1000-µL and 200-µL pipette tips. Dissociated cells were collected by centrifugation at 130 × g for 10 min at room temperature and seeded onto poly-D-lysine-coated culture plates in Neurobasal medium supplemented with 2 mM L-glutamine, N2 supplement, B27 supplement and 50 µg/mL penicillin-streptomycin (P/S; all from Gibco™). Half of the culture medium was replaced after 5 days and subsequently every 2 days. Neurons were used for experiments after 10–14 days in culture.

Primary astrocyte cultures were prepared from postnatal day 1–2 (P1-P2) C57BL/6 mice as previously described [24]. Briefly, whole brains were isolated, mechanically dissociated, and passed through a 70-µm cell strainer. Cells were seeded into T75 culture flasks and maintained at 37 °C in a humidified atmosphere containing 5% CO_2. The culture medium was replaced after 5 days and every 2 days thereafter. Mixed glial cultures were maintained for 14–21 days before purification. To obtain enriched astrocyte cultures, mixed glial cultures were shaken at 250 rpm for 4 h to remove loosely adherent microglia and oligodendrocyte lineage cells. The remaining astrocytes were detached using trypsin-EDTA (Gibco™), collected by centrifugation, and replated in Dulbecco's modified Eagle medium (DMEM; Gibco™) supplemented with 10% heat-inactivated fetal bovine serum (FBS; Gibco™) and 50 µg/mL P/S. All animal procedures were conducted in accordance with the National Institutes of Health Guide for the Care and Use of Laboratory Animals and were approved by the appropriate institutional animal care and use committee.

Transfection

Primary astrocytes were transfected with GFP (pCMV6-AC-GFP), human FUS P525L (pCMV6-AC-FUS-GFP; the P525L mutant was generated by site-directed mutagenesis), or human TDP-43 (pCMV6-AC-TDP-43-GFP) expression vectors (all from Origene Technologies) using Neon Transfection System (Invitrogen™) according to the manufacturer's instructions. At 2 days post-transfection, cells were treated with DHE (10 µM) or an equivalent concentration of EtOH (vehicle) for 24 h. A total experimental duration of 3 days post-transfection was selected to minimize transfection-associated background toxicity while allowing sufficient expression of the transgenes.

Nitric Oxide (NO) assay

Primary mouse astrocytes were stimulated with lipopolysaccharide (LPS; 100 ng/mL) and interferon-γ (IFN-γ; 10 U/mL) for 24 h. Human primary astrocytes were stimulated with interleukin-1β (IL-1β; 10 ng/mL), TNF-α (10 ng/mL), and IFN-γ (200 U/mL) for 48 h. Astrocytes were pretreated with DHE (10 µM) for 30 min prior to inflammatory stimulation. Following stimulation, culture supernatants were collected and nitrite levels were quantified using the Griess Reagent System (G2930; Promega) according to the manufacturer's instructions. Briefly, culture supernatants were mixed with the Griess reagents and incubated at room temperature for color development. Absorbance was measured at 540 nm using a microplate reader (Tecan). Nitrite concentrations were calculated from a sodium nitrite standard curve and expressed as µM nitrite.

Cytotoxicity assay

Cell viability was assessed using the Cell Counting Kit-8 (CCK-8; Enzo Life Sciences) according to the manufacturer's instructions. Briefly, 10 µL of CCK-8 reagent was added to each well, and cell were incubated at 37 °C for 2 h. Absorbance was measured at 450 nm using a microplate reader (Tecan). Cell viability was expressed as a percentage of the corresponding control group. All experiments were performed with three independent biological replicates.

For neuronal survival analysis, primary cortical neurons were labeled with a 5 µM CellTracker Green CMFDA dye (Invitrogen™) for 30 min according to the manufacturer's protocol. Following dye incubation, cells were washed and incubated with dye-free medium for 45 min. Fluorescent images were acquired using a fluorescence microscope. For quantification, images were collected from three randomly selected fields per sample, and CMFDA-positive cells were counted. Cell survival was expressed as a percentage of the corresponding control group.

Preparation of astrocyte-conditioned medium

To generate astrocyte-conditioned medium (ACM), primary astrocytes transfected with GFP, FUS P525L, or TDP-43 expression constructs were treated with DHE (10 µM) or EtOH (vehicle) for 24 h. Cells were subsequently washed twice with phosphate-buffered saline (PBS) and cultured in fresh DMEM for an additional 24 h. Conditioned medium was collected, centrifuged at 200 × g for

10 min to remove cellular debris, aliquoted, and stored at – 80 °C until use.

ACM-treatment of primary cortical neurons

Primary cortical neurons were exposed for 5 days to ACM derived from GFP-transfected astrocytes treated with EtOH (GFP ACM), FUS P525L-transfected astrocytes treated with EtOH (FUS P525L ACM), FUS P525L-transfected astrocytes treated with DHE (FUS P525L + DHE ACM), TDP-43-transfected astrocytes treated with EtOH (TDP-43 ACM), or TDP-43-transfected astrocytes treated with DHE (TDP-43 + DHE ACM). Following treatment, neuronal viability and survival were evaluated using the CCK-8 assay and CMFDA staining, respectively.

Quantitative reverse transcription polymerase chain reaction (RT-qPCR)

Total RNA was extracted from cultured cells and *Drosophila melanogaster* heads using TRIzol™ reagent (Invitrogen™). RNA samples were purified using the RNeasy Mini Kit (QIAGEN) according to the manufacturer's instructions. cDNA was synthesized from 50 ng of total RNA using the High Capacity cDNA Reverse Transcription Kit (Applied Biosystems) at 37 °C for 120 min. Quantitative RT-PCR was performed using TB Green® Premix Ex Taq™ (Tli RNaseH Plus) (Takara Bio Inc.) according to the manufacturer's protocol, on Applied Biosystems 7500 Real-Time PCR System (Applied Biosystems). Relative gene expression levels were normalized to *Gapdh* and *18 S rRNA* and calculated using the $2^{-\Delta\Delta Ct}$ method [25]. The primer sequences used in this study are listed in Table 1.

Immunoblot analysis

For total protein extraction, cultured cells were lysed in Cell Lysis Buffer (Cell Signaling Technology) supplemented with protease and phosphatase inhibitor cocktails (Roche). Samples were centrifuged at 14,000 × g for 30 min at 4 °C, and the resulting supernatants were collected for analysis. Protein concentrations were determined using the Pierce BCA Protein Assay Kit (Thermo Fisher Scientific™), according to the manufacturer's instructions. Next, the cell lysate were mixed with 4× Bolt™ LDS Sample Buffer (Invitrogen™) and 10× Bolt™ Sample Reducing Agent buffer (Invitrogen™), and heated at 95 °C for 5 min. Adult *D. melanogaster* heads were homogenized using disposable homogenizers in a mixture of 4× Bolt™ LDS Sample Buffer (Invitrogen™) and 10× Bolt™ Sample Reducing Agent (Invitrogen™), and subsequently heated at 95 °C for 5 min. Samples were centrifuged at 14,000 × g for 30 min at 4 °C, and the resulting supernatants were collected for analysis. Equal amounts of protein were separated by SDS-PAGE using Bolt™ 4–12% Bis-Tris Plus Gels (Invitrogen™) or

Table 1 Primer sequences used for RT-qPCR

Gene	Forward (5′ to 3′)	Reverse (5′ to 3′)
Human		
IL1B	ATGCACCTGTACGATCACTG	ACAAAGGACATGGAGAACACC
IL6	CCACTCACCTCTTCAGAACG	CATCTTTGGAAGGTTCAGGTTG
TNF	ACTTTGGAGTGATCGGCC	GCTTGAGGGTTTGCTACAAC
18 S rRNA	CGGCGACGACCATTCGAAC	GAATCGAACCCTGATTCCCCGTC
Mouse		
Cxcl10	GATGACGGGCCAGTGAGAA	GCTCGCAGGGATGATTTCAA
Ccl3	GATTCCACGCCAATTCATCG	TTCAGTTCCAGGTCAGTGATG
Ccl19	GCTGGTTCTCTGGACCTTC	CCTGCAGCCATCTTCATTAAG
Cat	CTCGTTCAGGATGTGGTTTTC	CTTTGCCTTGGAGTATCTGGTG
Nqo1	TGAAGAAGAGAGGATGGGAGG	GATGACTCGGAAGGATACTGAAAG
Hmox1	ACAGAGGAACACAAAGACCAG	GTGTCTGGGATGAGCTAGTG
Sod2	TGCTCTAATCAGGACCCATTG	CATTCTCCCAGTTGATTACATTCC
Il1b	TTGACGGACCCCAAAAGATG	TGGACAGCCCAGGTCAAAG
Il6	CCACGGCCTTCCCTACTTC	TTGGGAGTGGTATCCTCTGTGA
Tnf	TCCAGGCGGTGCCTATGT	GCCCCTGCCACAAGCA
Nos2	GGATCTTCCCAGGCAACCA	TCCACAACTCGCTCCAAGATT
18 S rRNA	TTCGTATTGCGCCGCTAGA	CTTTCGCTCTGGTCCGTCTT
Drosophila		
AttC	CCACCCTGGGCTACAACAAT	GGCGTATGGGTTTTGGTCAGT
DptB	GCCTGGGCTTATCCCTATCC	AGTGGTTCAGGCTGCAGATTC
Dif	CGATTCCGGGCATGAACT	CGATGGTGGGAAAGGTCTTG
Rel	AACCGCCGCGAGTTGTC	ACGCTCTGTCTCCTGATGCA
Gapdh	GGCTGGCATTTCGCTGAA	CCGAACTCGTTGTCGTACCA

NuPAGE™ 3–8% Tris-Acetate Protein Gels (Invitrogen™) and transferred onto polyvinylidene difluoride (PVDF) membranes using the iBlot™ 2 Transfer Stacks and iBlot™ 2 Dry Blotting System (Invitrogen™) according to the manufacturer's instructions. Membranes were blocked in 5% skim milk and incubated sequentially with primary antibodies and HRP-conjugated secondary antibodies. Immunoreactive bands were visualized using ECL Prime Western Blotting Detection Reagents (Cytiva). Densitometric analysis was performed using Fusion-FX software (Vilber Lourmat). Data were derived from three independent biological experiments.

Nuclear and cytoplasmic fractionation

Primary astrocytes expressing FUS P525L or TDP-43 were fractionated using the NE-PER™ Nuclear and Cytoplasmic Extraction Reagents Kit (Thermo Scientific™) according to the manufacturer's protocol. Briefly, cells were sequentially extracted with Cytoplasmic Extraction Reagents I and II (CER I and CER II), and cytoplasmic fractions were collected following centrifugation at 16,000 × g for 5 min at 4 °C. The remaining pellets were resolubilized in Nuclear Extraction Reagent (NER) and incubated according to the manufacturer's instructions. Following centrifugation at 16,000 × g for 10 min at 4 °C, nuclear extracts were collected. Samples were mixed with 4× Bolt™ LDS Sample Buffer and 10× Bolt™ Sample Reducing Agent and heated at 95 °C for 5 min prior to immunoblot analysis.

Preparation of soluble and insoluble protein fractions

Cultured cells and adult *D. melanogaster* heads were homogenized in Cell Lysis Buffer supplemented with protease and phosphatase inhibitor cocktails. Homogenates were sonicated and centrifuged at 100,000 × g for 30 min at 4 °C. The resulting supernatants were collected as the soluble protein fractions. Pellets were washed once with lysis buffer containing inhibitors, and centrifuged at 100,000 × g for 30 min at 4 °C. The final pellet was resuspended in 2% dodecyl sulfate (SDS) and sonicated to obtain the insoluble protein fractions. Soluble and insoluble fractions were mixed with 4×Bolt LDS Sample Buffer and 10×Bolt Sample Reducing Agent, heated at 95 °C for 5 min, and analyzed by immunoblotting.

Enzyme-linked immunosorbent assay (ELISA)

Protein concentrations in ACM were quantified using DuoSet® ELISA Development Systems (R&D Systems) according to the manufacturer's protocol. Briefly, 96-well plates were coated with the capture antibodies and subsequently blocked. Samples and recombinant cytokine or chemokine standards were then added to the wells. Bound analytes were detected using biotinylated detection antibodies followed by streptavidin-HRP. Color development was achieved using the recommended substrate solution, and absorbance was measured at 450 nm with wavelength correction at 540 nm using a microplate reader (Tecan).

Mitochondrial activity assay

Neuronal mitochondrial function was assessed using the Seahorse XF Cell Mito Stress Test. Primary cortical neurons were seeded in XF24-cell culture microplates (Agilent Technologies) and exposed to GFP ACM, FUS P525L ACM, or FUS P525L + DHE ACM for 5 days. Following treatment, cells were washed twice with Seahorse XF Base Medium supplemented with 2 mM L-glutamine, 10 mM D-glucose, and 1 mM sodium pyruvate (pH 7.4) and incubated at 37 °C in a non-CO2 incubator for 1 h. Mitochondrial respiration was measured using the SeahorseXF Cell Mito Stress Test Kit (Agilent Technologies) according to the manufacturer's instructions on an XF24 Extracellular Flux Analyzer (Agilent Technologies). For the assay, sensor cartridges were hydrated, treated with oligomycin (2 μM), carbonyl cyanide 4-(trifluoromethoxy) phenylhydrazone (FCCP; 1 μM), and antimycin A plus rotenone (0.5 μM each). Basal respiration, ATP-linked respiration, maximal respiration, and spare respiratory capacity were calculated as previously described [26]. Measurements were obtained from five technical replicate wells per condition within each independent experiment. To normalize oxygen consumption rate (OCR) values, cells were lysed following Seahorse analysis. Briefly, plates were centrifuged at 280 × g for 5 min, washed twice with PBS, and lysed in Cell Lysis Buffer (Cell Signaling Technology). Protein concentrations were determined using the Pierce BCA Protein Assay Kit, and OCR values were normalized to that of total cellular protein content.

Human participants

Primary dermal fibroblasts were obtained from a patient with ALS carrying a heterozygous *FUS* p.G504Wfs*12 mutation (34-year-old female) and from an age-matched healthy female control (35-years-old) as previously described [27].

Human primary fibroblasts

Primary dermal fibroblasts were established from skin biopsy specimens obtained from the ALS patient carrying the *FUS* p.G504Wfs*12 mutation and the healthy control (HC) donor. Cells were cultured in DMEM (Gibco™) supplemented with 10% heat-inactivated FBS, 1× MEM non-essential amino acids (MEM-NEAA; Gibco), and 100 μg/mL Normocin (InvivoGen). Cells were maintained at 37 °C in a humidified atmosphere containing 5% CO_2. Passage-matched fibroblasts between passages 7 and 10 were used for all experiments.

Human primary astrocytes

Primary human astrocytes (1800; ScienCell Research Laboratories) were cultured in poly-L-lysine-coated flasks using Astrocyte Medium (ScienCell) according to the manufacturer's instructions. Cells were maintained at 37 °C in a humidified incubator containing 5% CO_2 under mycoplasma-free conditions and passaged upon reaching approximately 90% confluence. Cells at passages less than 5 were used for all experiments.

Drosophila strains

D. melanogaster stocks were maintained on standard cornmeal–agar medium at 24 °C unless otherwise indicated. The UAS-FUS P525L transgenic line was generously provided by Dr. Nancy M. Bonini (University of Pennsylvania, Philadelphia, PA, USA). The UAS-TDP-43 transgenic line has been described previously [28]. The glial driver line repo-GAL4 and the combined genotype repo-GAL4/UAS-TDP-43 have been reported previously [29]. To induce glial expression of disease-associated proteins, virgin females carrying UAS- FUS P525L or UAS-TDP-43 transgenes were crossed with males carrying the repo-Gal4 driver, resulting in progeny expressing FUS P525L or TDP-43 throughout the glial cell population.

Drosophila lifespan and climbing assays

Lifespan and climbing assays were performed using male progeny generated from crosses between repo-GAL4 driver flies and either UAS-FUS P525L or UAS-TDP-43 flies. Newly eclosed male flies (0–1 day old) were collected and transferred to vials containing standard fly food supplemented with DHE (10 μM) or vehicle control. Flies were maintained at a density of 23–25 flies per vial, and experiment were conducted with at least 98 flies per genotype and treatment condition. Mortality was recorded daily, and flies were transferred to vials containing fresh food every other day. Climbing performance was assessed using a negative geotaxis assay as previously described [30]. All experiments were independently repeated twice.

Participants and clinical assessment

This study was approved by the Institutional Review Board of Kyungpook National University Chilgok Hospital (KNUMC-2023–01-036-001), and written informed consent was obtained from all participants prior to enrollment. A total of 30 patients diagnosed with amyotrophic lateral sclerosis (ALS) and 44 HCs were recruited at the Department of Neurology, Kyungpook National University Chilgok Hospital between 2020 and 2023. The diagnosis of ALS was established according to the revised El Escorial criteria. Clinical demographic information of ALS patients, including age, age at symptom onset, and disease duration, was collected. Functional status was evaluated using the ALS Functional Rating Scale–Revised (ALSFRS-R). HC had no history of neurological or systemic disorders.

Plasma sample collection

Peripheral blood (10 mL) was collected from each participant into EDTA-coated blood collection tubes (BD Vacutainer) and gently inverted to ensure adequate mixing with the anticoagulant. Samples were processed within 30 min of collection and centrifuged at 3,000 × g for 10 min at room temperature. Plasma was carefully collected, aliquoted into sterile 2.0-mL microcentrifuge tubes, and stored at – 80 °C until analysis.

Olink target 48 cytokine panel analysis

Plasma protein profiling was performed using the Olink Target 48 Cytokine panel (Olink Proteomics) according to the manufacturer's instructions. Briefly, pairs of oligonucleotide-labeled antibodies bind to their respective target proteins, allowing proximity-dependent hybridization of the attached oligonucleotides. This proximity extension assay generates unique DNA reporter sequences that are subsequently amplified and quantified by real-time qPCR using the Olink Signature Q100 system (Olink Proteomics).

Neurofilament light chain (NfL) measurements

Plasma NfL concentrations were quantified using the NF-Light V2 Advantage Kit (104073; Quanterix) on the fully automated single-molecule array (Simoa) HD-X Analyzer according to the manufacturer's instructions. Plasma samples were diluted 1:4 prior to analysis. The assay uses antibody-coated paramagnetic beads to capture target proteins, followed by incubation with a biotinylated detection antibody and streptavidin-β-galactosidase conjugate. Signal was generated through hydrolysis of the resorufin β-D-galactopyranoside (RGP) substrate, and analyte concentrations were calculated from the average enzyme per bead (AEB). All samples were analyzed in duplicate, and the mean value was used for subsequent statistical analyses.

Statistical analysis

Data are presented as the mean ± standard deviation (SD) unless otherwise indicated. Statistical analyses were performed using GraphPad Prism (GraphPad Software) and VassarStats. Comparisons between two groups were conducted using an unpaired two-tailed Student's *t*-test or Welch's *t*-test, as appropriate. Comparisons among multiple groups were performed using one-way analysis of variance (ANOVA) followed by Tukey's multiple-comparisons test. Differences were considered statistically significant at $p < 0.05$. Statistical significance is

indicated as follows: $^{*}p < 0.05$, $^{**}p < 0.005$, $^{***}p < 0.001$, and $^{****}p < 0.0001$; NS, not significant.

Results

DHE suppressed NF-κB-dependent inflammatory signaling and reduced FUS protein accumulation in FUS P525L-expressing astrocytes

Combined LPS and IFN-γ stimulation promotes astrocyte activation and induces robust inflammatory responses characterized by increasing the expression of pro-inflammatory mediators, including nitric oxide (NO) and reactive oxygen species (ROS) [31]. To confirm anti-inflammatory activity of DHE in primary mouse astrocytes, inflammatory responses was induced using LPS and IFN-γ, followed by DHE treatment in our study. Treatment with DHE (10 μM) significantly reduced the nitrite production induced by LPS/IFN-γ stimulation without affecting cell viability (Fig. 1A).

To determine whether these anti-inflammatory effects were also observed in human astrocytes, primary human astrocytes were stimulated with a cytokine cocktail consisting of IL-1β, TNF-α, and IFN-γ. Cytokine stimulation significantly increased nitrite production, which was attenuated by DHE treatment (Supplementary Fig. 1A). In addition, DHE reduced the expression of pro-inflammatory genes, including *IL1B*, *IL6*, and *TNF* in human primary astrocytes (Supplementary Fig. 1B).

Expression of mutant FUS in astrocytes promotes neurotoxicity via activating the NF-κB pathway [21], whereas DHE inhibits NF-κB signaling via modulating IKKβ activity [7]. We therefore examined whether DHE regulates NF-κB signaling in astrocytes expressing FUS P525L. Overexpression of FUS P525L increased phosphorylation of IKKα/β (Ser176/180), IκBα (Ser32/Ser36), and NF-κB p65 (Ser536) compared with that in GFP-transfected controls (Fig. 1b). DHE treatment significantly attenuated

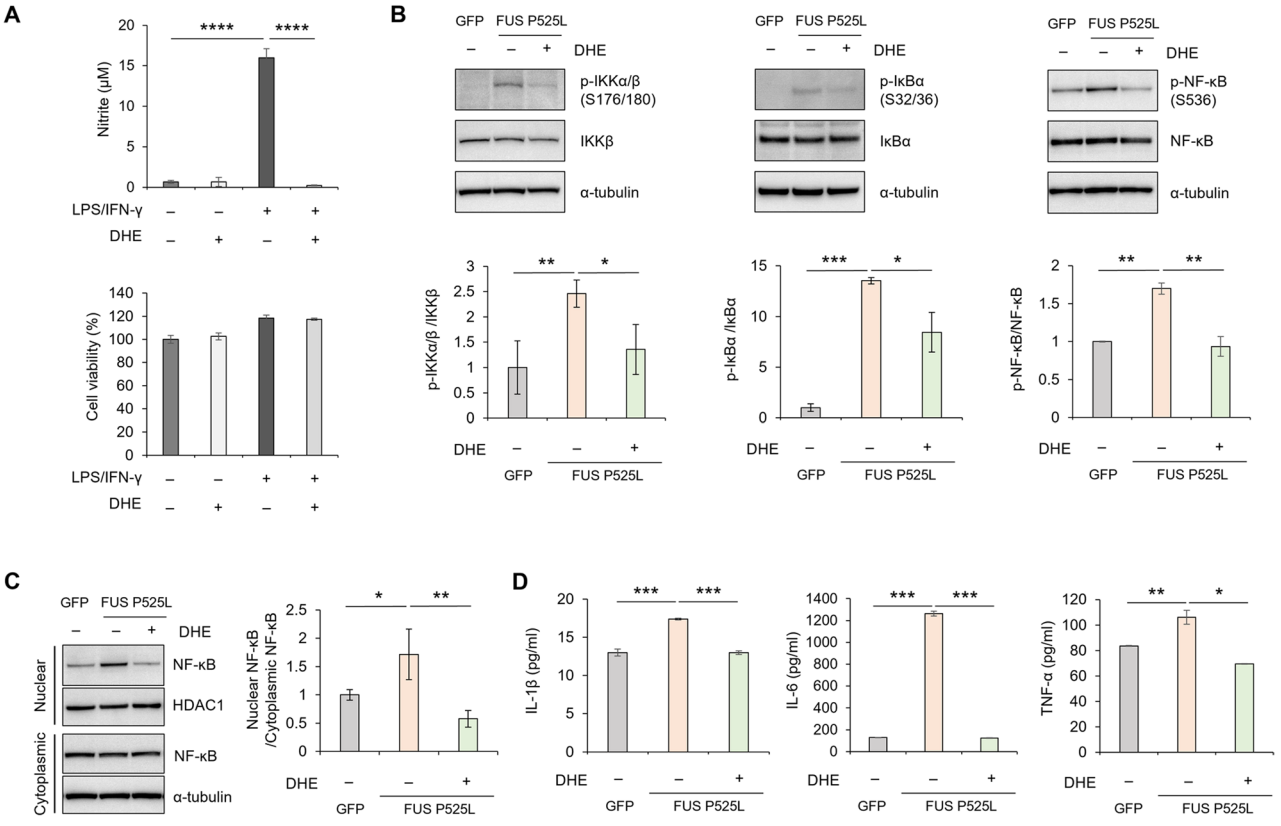

Fig. 1 DHE suppresses NF-κB signaling and inflammatory mediator production in FUS P525L-expressing astrocytes. **A** Primary mouse astrocytes were stimulated with LPS (100 ng/mL) and IFN-γ (10 U/mL) in the presence or absence of DHE (10 μM; 30 min pretreatment). NO production and cell viability were measured after 24 h using Griess assay and CCK-8 assay, respectively. **B** Primary astrocytes were transfected with GFP or FUS P525L expression constructs and treated with DHE (10 μM) for 24 h. Immunoblot analysis was performed to assess activation of the canonical NF-κB signaling pathway. Representative immunoblots and quantification of phospho-IKKα/β (Ser176/180), phospho-IκBα (Ser32/36), and phospho-NF-κB p65 (Ser536) normalized to their corresponding total protein levels are shown. **C** Cytoplasmic and nuclear fractions were isolated from GFP- or FUS P525L-expressing astrocytes following DHE treatment. NF-κB p65 levels were assessed by immunoblotting. α-tubulin and HDAC1 were used as cytoplasmic and nuclear loading controls, respectively. **D** ACM was collected from GFP ACM, FUS P525L ACM, and FUS P525L + DHE ACM. Secreted IL-1β, IL-6, and TNF-α levels were quantified by ELISA. Data are presented as mean ± SD from three independent experiments ($n = 3$). Statistical analysis was performed using one-way ANOVA followed by Tukey's multiple-comparisons test. $^{*}p < 0.05$; $^{**}p < 0.005$; $^{***}p < 0.001$; $^{****}p < 0.0001$

phosphorylation of all three signaling components. Consistent with these findings, FUS P525L expression promoted nuclear accumulation of NF-κB p65, whereas DHE markedly reduced NF-κB nuclear translocation (Fig. 1C).

To determine whether inhibition of NF-κB signaling translated into reduced inflammatory output, we quantified secreted inflammatory mediators in ACM. Concentrations of IL-1β, IL-6, and TNF-α significantly increased in ACM derived from FUS P525L-expressing astrocytes relative to those in GFP controls. Moreover, DHE treatment significantly reduced the secretion of all three inflammatory mediators (Fig. 1D).

Mutations affecting the C-terminal nuclear localization signal of FUS are among the most common causes of FUS-associated ALS. The P525L variant is strongly associated with aggressive juvenile-onset disease and promotes pathological cytoplasmic accumulation of FUS protein [32]. We therefore investigated whether DHE influences treatment affects the pathological aggregation of FUS P525L protein accumulation in, we first lysed total protein and fractionated it into soluble and insoluble fractions, as well as nuclear and cytoplasmic fractions, from astrocytes overexpressing expressing FUS P525L. DHE treatment reduced total FUS protein levels in FUS P525L-expressing astrocytes (Fig. 2A) as well as significantly reduced both soluble and insoluble FUS protein fractions (Fig. 2B). Similarly, DHE decreased cytoplasmic FUS accumulation, whereas nuclear FUS levels were not significantly altered (Fig. 2C).

Collectively, these findings indicate that DHE suppresses NF-κB–dependent inflammatory signaling and inflammatory mediator secretion while simultaneously reducing pathological FUS protein accumulation in FUS P525L-expressing astrocytes.

DHE attenuated astrocyte-mediated neurotoxicity and mitochondrial dysfunction induced by FUS P525L

To determine whether DHE modulates astrocyte-mediated neurotoxicity induced by FUS P525L, primary cortical neurons were exposed to ACM derived from GFP-transfected astrocytes, FUS P525L-expressing astrocytes, or DHE-treated FUS P525L-expressing astrocytes. Exposure to ACM from FUS P525L-expressing astrocytes significantly reduced neuronal viability compared

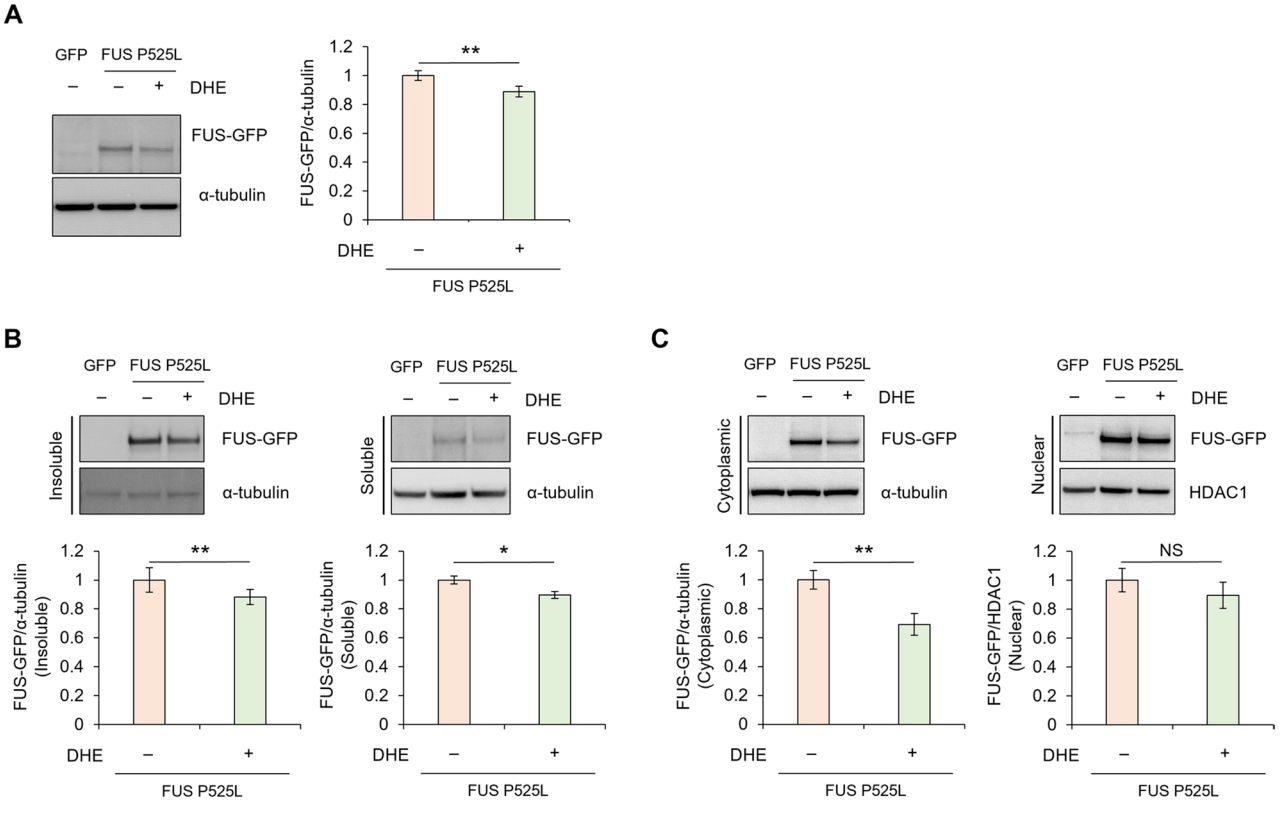

Fig. 2 DHE reduces pathological FUS protein accumulation in FUS P525L-erexpressing astrocytes. **A** Primary astrocytes expressing FUS P525L were treated with DHE (10 μM) for 24 h. Total FUS protein levels were analyzed by immunoblotting and normalized to α-tubulin. **B** Soluble and insoluble protein fractions were isolated from GFP- or FUS P525L-expressing astrocytes following DHE treatment and normalized to α-tubulin. **C** Cytoplasmic and nuclear fractions were prepared from GFP- or FUS P525L-expressing astrocytes treated with DHE. FUS protein levels were analyzed by immunoblotting. α-tubulin and HDAC1 served as cytoplasmic and nuclear loading controls, respectively. Data are presented as mean ± SD from three independent experiments ($n = 3$). Statistical analysis was performed using one-way ANOVA followed by Tukey's multiple-comparisons test. *$p < 0.05$; **$p < 0.005$; NS, not significant

with exposure to ACM from GFP-transfected astrocytes. In contrast, ACM derived from DHE-treated FUS P525L-expressing astrocytes significantly attenuated neuronal toxicity (Fig. 3A). The neuroprotective effect of DHE was further confirmed by CMFDA staining. Neurons exposed to FUS P525L ACM exhibited a marked reduction in the number of CMFDA-positive cells, whereas treatment with ACM from DHE-treated FUS P525L-expressing astrocytes significantly increased neuronal survival (Fig. 3B). Because mitochondrial dysfunction is a key feature of ALS pathogenesis, we next investigated whether astrocytic FUS P525L expression impairs neuronal mitochondrial respiration. Primary cortical neurons treated with ACM were subjected to Seahorse extracellular flux analysis. Exposure to FUS P525L ACM significantly reduced basal respiration ATP-linked respiration, maximal respiration, and spare respiratory capacity compared with GFP ACM (Fig. 3C). Importantly, ACM derived from DHE-treated FUS P525L-expressing astrocytes significantly restored all four mitochondrial respiration parameters.

Collectively, these findings demonstrate that DHE reduces astrocyte-mediated neurotoxicity and alleviates neuronal mitochondrial dysfunction induced by FUS P525L-expressing astrocytes.

DHE ameliorated glial FUS P525L-induced behavioral deficits and inflammatory gene expression in Drosophila

To evaluate the in vivo effects of DHE on FUS-mediated toxicity, we used *D. melanogaster* model expressing human FUS P525L in glial cells. Flies expressing FUS P525L exhibited progressive impairments in climbing performance and reduced lifespan compared with control flies. DHE treatment significantly improved locomotor function and extended survival in FUS P525L-expressing flies (Fig. 4A, B). As DHE suppressed NF-κB signaling in mammalian astrocytes, we next examined the expression of genes associated with the Toll and immune deficiency (IMD) pathways, which represent major NF-κB-related immune signaling pathways in *Drosophila*. The expression of the antimicrobial peptide genes *AttC* and *DptB*, as well as the NF-κB-related transcription factors *Dif*

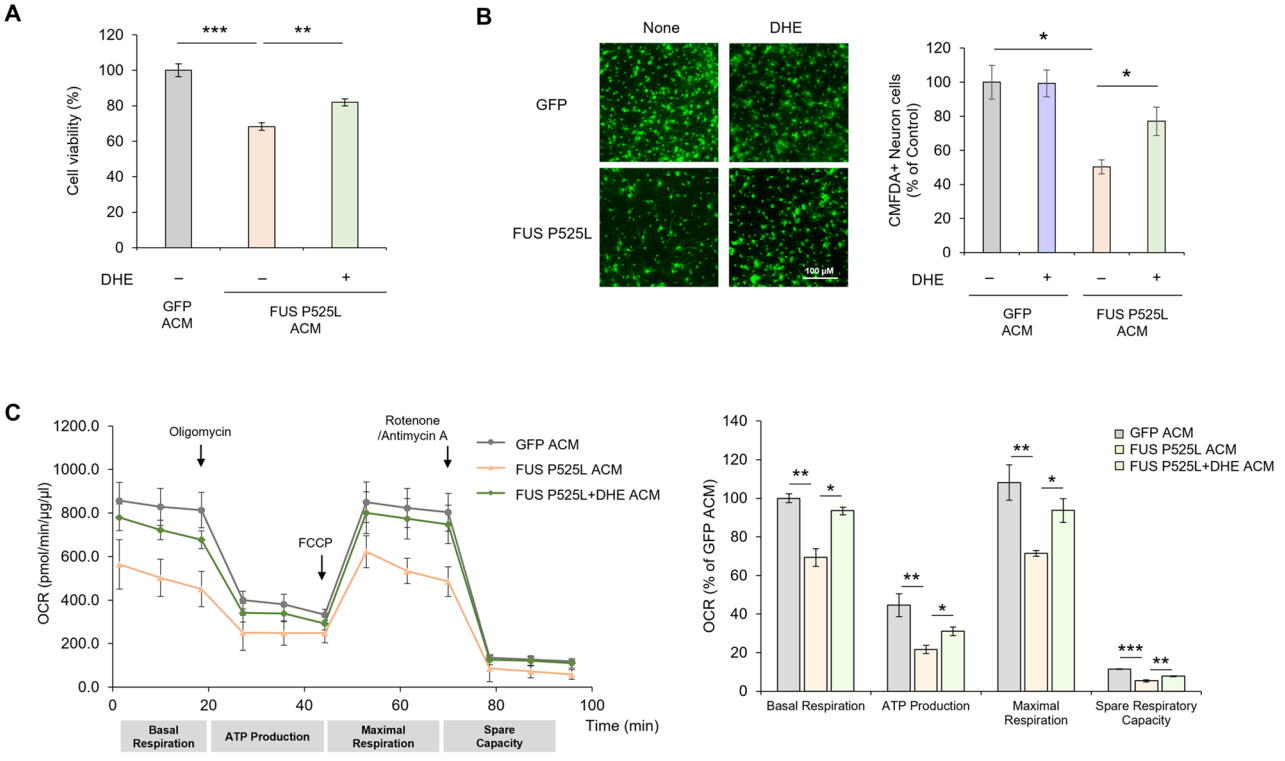

Fig. 3 DHE attenuates astrocyte-mediated neurotoxicity and mitochondrial dysfunction induced by FUS P525L. **A** Primary astrocytes expressing FUS P525L were treated with DHE (10 μM) for 24 h, and ACM was collected. Primary cortical neurons were exposed to GFP ACM, FUS P525L ACM, or FUS P525L + DHE ACM for 5 days. Neuronal viability was assessed using the CCK-8 assay. **B** Primary cortical neurons were treated as described in A, followed by CMFDA to evaluate neuronal survival. Representative images and quantification of CMFDA-positive cells are shown. Cell numbers are expressed relative to the GFP ACM control group. Scale bar, 100 μm. **C** Primary cortical neurons cultured in XF24 microplates were exposed to GFP ACM, FUS P525L ACM, or FUS P525L + DHE ACM for 5 days. Mitochondrial respiration was assessed using the Seahorse XF Cell Mito Stress Test. Representative OCR, ATP-linked respiration, and spare respiratory capacity are shown. The OCR values were normalized to total cellular protein content. Data are presented as mean ± SD (A, B) or mean ± SEM (C), from three independent experiments ($n = 3$). Statistical analysis was performed using one-way ANOVA followed by Tukey's multiple-comparisons test. *$p < 0.05$; **$p < 0.005$; ***$p < 0.001$

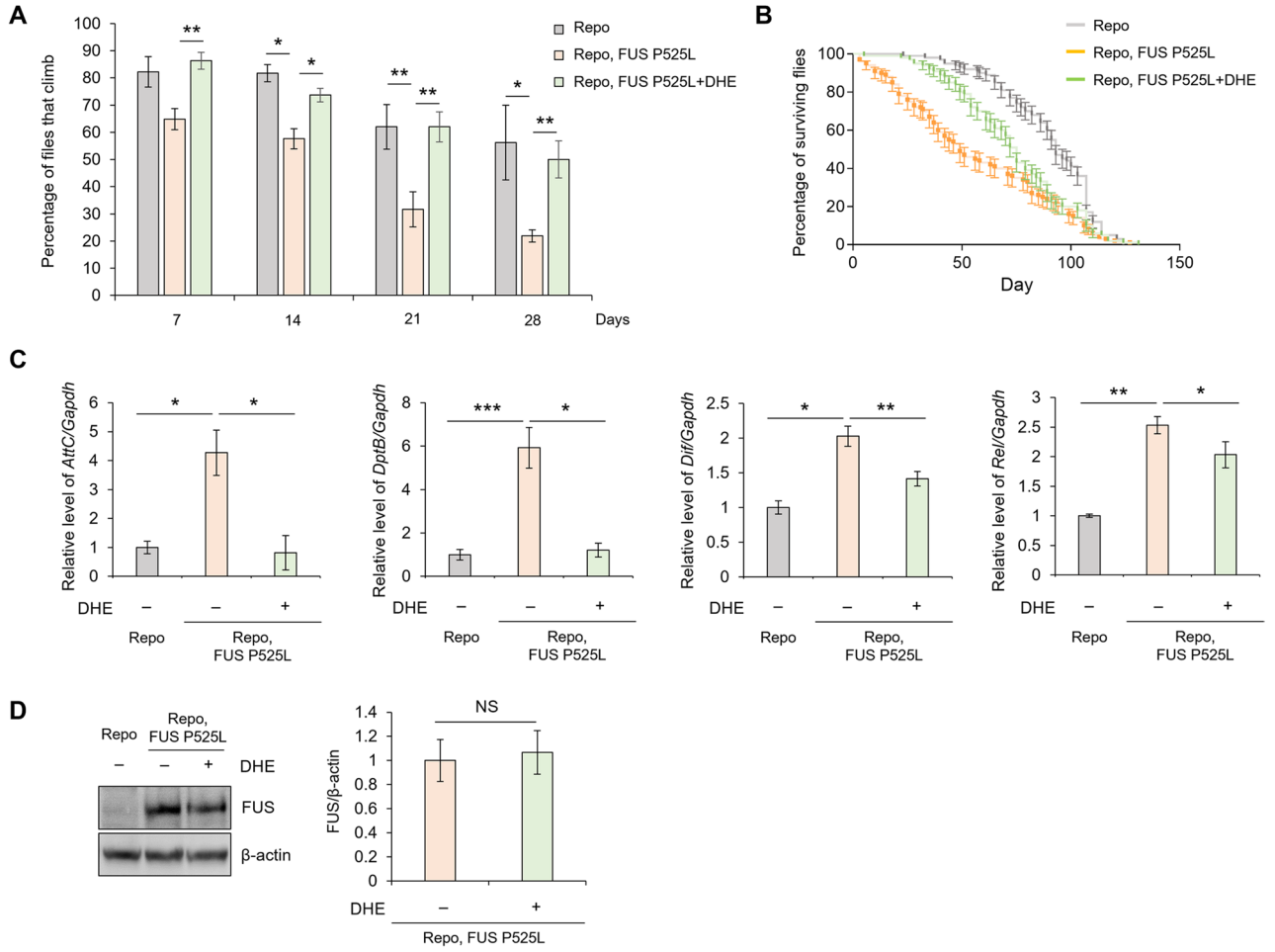

Fig. 4 DHE ameliorates glial FUS P525L-induced behavioral deficits and inflammatory gene expression in *Drosophila*. **A** Climbing performance of control flies (repo-Gal4) and flies expressing glial FUS P525L in the presence or absence of DHE treatment. Climbing activity was assessed at the indicated time points. **B** Survival analysis of control flies and flies expressing glial FUS P525L with or without DHE treatment. **C** Quantitative RT-qPCR analysis of *AttC*, *DptB*, *Dif*, and *Rel* expression in adult fly heads. RNA was isolated from 25 flies per genotype collected from four independent vials. Expression levels were normalized to *Gapdh*. **D** Immunoblot analysis of total FUS protein levels in adult fly heads. For each genotype, four independent vials of 21 flies each were used; heads from the 21 flies in each vial were collected and pooled to prepare one protein lysate, yielding four independent lysates per condition that were loaded for immunoblotting. Lysates were prepared from flies expressing glial FUS P525L with or without DHE treatment. β-actin was used as a loading control. Data are presented as mean ± SEM (A, B, and D) or mean ± SD (C). For climbing and lifespan analyses, flies were maintained at 23–25 flies per vial with four independent vials per condition. Statistical significance was determined using one-way ANOVA followed by Tukey's multiple-comparisons test or Student's *t*-test, as appropriate. *$p < 0.05$; **$p < 0.005$; ***$p < 0.001$; NS, not significant

and *Rel*, was significantly increased in flies expressing glial FUS P525L. DHE treatment significantly reduced the expression of all four genes (Fig. 4C). To determine whether DHE also affected FUS protein levels in vivo, we analyzed total FUS expression in adult fly heads. In contrast to the findings in primary astrocytes, DHE treatment did not significantly alter total FUS protein levels in flies expressing glial FUS P525L (Fig. 4D). Consistently, fractionation of fly head lysates revealed no significant changes in either soluble or insoluble FUS protein levels following DHE treatment (Supplementary Fig. 2).

Together, these findings demonstrate that DHE alleviates glial FUS P525L-induced behavioral deficits and suppresses inflammatory gene expression in vivo without significantly altering FUS protein accumulation.

DHE reduced FUS accumulation and NF-κB activation in FUS-ALS patient-derived fibroblasts

To evaluate the effects of DHE in a patient-derived disease model, fibroblasts obtained from an HC donor and a patient with FUS-associated ALS carrying the *FUS* p.G504Wfs*12 mutation were subjected to sodium arsenite ($NaAsO_2$)-induced cellular stress. $NaAsO_2$ is a well-established inducer of oxidative stress and stress granule formation and has been widely used to model stress-associated cellular responses [27, 33–35]. We first examined the effects of DHE on FUS protein

levels under stress conditions. $NaAsO_2$ treatment increased FUS protein accumulation in fibroblasts derived from the FUS-ALS patient compared with control fibroblasts. DHE treatment significantly attenuated the stress-induced increase in FUS protein levels (Fig. 5A). As NF-κB signaling was modulated by DHE in primary astrocytes, we next assessed NF-κB activation in patient-derived fibroblasts. $NaAsO_2$ treatment increased phosphorylation of NF-κB p65 at Ser536 in FUS-ALS fibroblasts, whereas DHE treatment significantly reduced NF-κB phosphorylation (Fig. 5B). These findings demonstrate that DHE suppresses stress-induced FUS accumulation and NF-κB activation in FUS-ALS patient-derived fibroblasts.

DHE suppressed TDP-43-induced NF-κB activation, astrocyte-mediated neurotoxicity, and behavioral deficits

As both mutant FUS and TDP-43 promote astrocyte-mediated neurotoxicity through the NF-κB signaling [21, 36], we next examined whether DHE exerts similar effects in a TDP-43 model. An earlier investigation demonstrated that overexpression of TDP-43 in astrocytes triggers inflammation via the NF-κB pathway, leading to the release of pro-inflammatory proteins that can eventually cause neurodegeneration [36].

Primary astrocytes expressing TDP-43 exhibited significantly increased phosphorylation of NF-κB p65 at Ser536 compared with that in GFP-transfected controls. DHE treatment markedly reduced TDP-43-induced NF-κB phosphorylation (Fig. 6A). Consistent with these

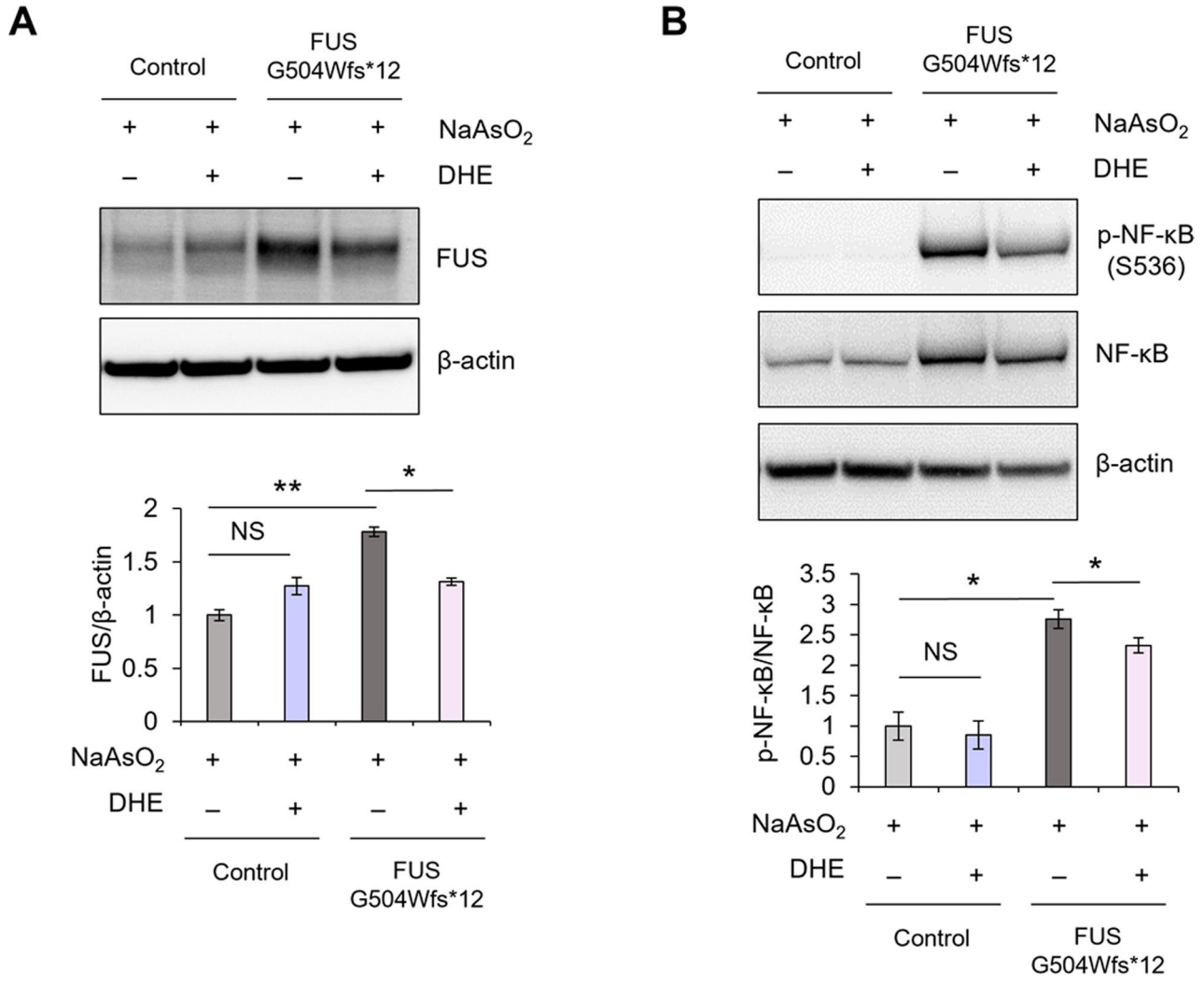

Fig. 5 DHE reduces FUS accumulation and NF-κB activation in FUS-ALS patient-derived fibroblasts. **A** Primary fibroblasts derived from a HC donor and a patient carrying the *FUS* p.G504Wfs*12 mutation were pretreated with DHE (10 μM) for 30 min and subsequently exposed to sodium arsenite ($NaAsO_2$; 0.5 mM) for 12 h. FUS protein levels were analyzed by immunoblotting and normalized to β-actin. **B** NF-κB activation was assessed by immunoblotting for phospho-NF-κB p65 (S536) and total NF-κB p65. Phosphorylated NF-κB was levels are presented relative to total NF-κB. Data are presented as mean ± SEM from three independent experiments ($n = 3$). Statistical analysis was performed using one-way ANOVA followed by Tukey's multiple-comparisons test. *$p < 0.05$; **$p < 0.005$; NS, not significant

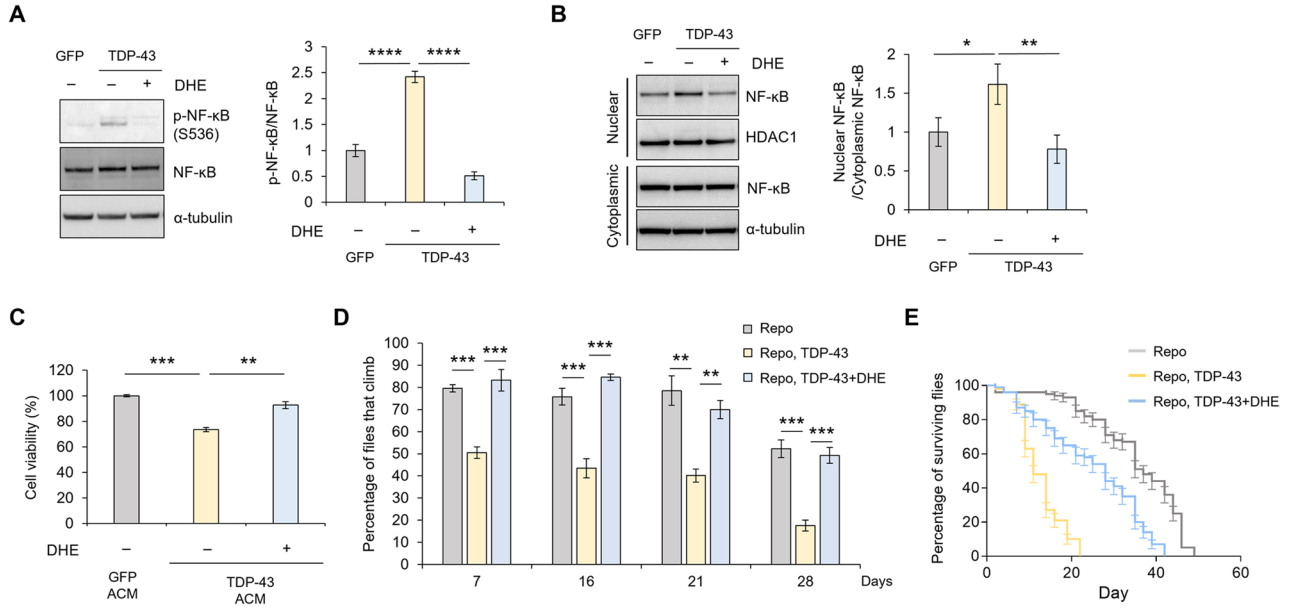

Fig. 6 DHE suppresses TDP-43-induced NF-κB activation, astrocyte-mediated neurotoxicity, and behavioral deficits. **A** Primary astrocytes were transfected with GFP or TDP-43 expression constructs and treated with DHE (10 μM) for 24 h. Immunoblot analysis was performed to assess NF-κB activation by measuring phospho-NF-κB p65 (S536) and total NF-κB p65 levels. Quantification is presented as the ratio of phospho-NF-κB to total NF-κB. **B** Cytoplasmic and nuclear fractions were isolated from TDP-43-expressing astrocytes following DHE treatment. NF-κB p65 levels were analyzed by immunoblotting. α-tubulin and HDAC1 were used as cytoplasmic and nuclear loading controls, respectively. Quantification is presented as ratio of nuclear to cytoplasmic NF-κB. **C** ACM was collected from GFP ACM, TDP-43 ACM, and TDP-43 + DHE ACM. Primary cortical neurons were exposed to ACM for 4 days, and neuronal viability was assessed using the CCK-8 assay. **D** Climbing performance of control flies (repo-GAL4) and flies expressing glial TDP-43 in the presence or absence of DHE treatment. **E** Survival analysis of control flies and flies expressing glial TDP-43 with or without DHE treatment. Data are presented as mean ± SD (A–C) or mean ± SEM (D, E). Cellular experiments (A–C) were performed independently three times ($n = 3$). For climbing and lifespan analyses, flies were maintained at 23–25 flies per vial with four independent vials per condition. Statistical significance was determined using one-way ANOVA followed by Tukey's multiple-comparisons test. *$p < 0.05$; **$p < 0.005$; ***$p < 0.001$; ****$p < 0.0001$

findings, cytoplasmic and nuclear fractionation demonstrated enhanced nuclear accumulation of NF-κB in TDP-43-expressing astrocytes, whereas DHE treatment significantly suppressed NF-κB nuclear translocation (Fig. 6B). To determine whether modulation of NF-κB signaling affected astrocyte-mediated neurotoxicity, primary cortical neurons were exposed to ACM derived from GFP-transfected astrocytes, TDP-43-expressing astrocytes, or DHE-treated TDP-43-expressing astrocytes. ACM from TDP-43-expressing astrocytes significantly reduced neuronal viability, whereas ACM derived from DHE-treated TDP-43-expressing astrocytes significantly attenuated neuronal toxicity (Fig. 6C).

We next evaluated the effects of DHE in a *Drosophila* model expressing human TDP-43 in glial cells. Consistent with our previous observations [36], glial TDP-43 expression caused progressive impairments in climbing performance and reduced lifespan compared with control flies, whereas DHE treatment significantly improved locomotor function and extended survival in TDP-43-expressing flies (Fig. 6D, E). Together, these findings demonstrate that DHE suppresses TDP-43-induced NF-κB activation and astrocyte-mediated neurotoxicity and ameliorates behavioral deficits in vivo.

DHE-responsive inflammatory mediators were elevated in ALS patient plasma and induced by FUS and TDP-43 in astrocytes

As DHE suppressed NF-κB activation in both FUS and TDP-43 models, we next examined the expression of downstream inflammatory mediators. Overexpression of either FUS P525L or TDP-43 in primary astrocytes significantly increased the expression of *Il1b*, *Il6*, *Tnf*, and *Nos2*, whereas DHE treatment markedly reduced the expression of all four genes (Supplementary Fig. 3).

To determine whether inflammatory mediators identified in our cellular models were also altered in patients with ALS, we analyzed plasma samples from 30 patients with sporadic ALS (sALS) and 44 HCs. Consistent with previous studies, plasma NfL concentrations were significantly elevated in patients with ALS compared with HCs (Table 2), supporting the clinical relevance of the cohort. Plasma inflammatory proteins were subsequently profiled using the Olink Target 48 Cytokine panel. Among the analytes examined, CXCL10, CCL3, and CCL19 were significantly elevated in ALS plasma samples relative to HCs (Fig. 7A; Table 2). We next investigated whether these inflammatory mediators were also induced in our astrocyte models. Overexpression of either FUS P525L or

Table 2 Clinical and biomarker profile of study participants

	HC (*n* = 44)	ALS (*n* = 30)	*p* value
Age (years)	67.64 ± 8.41	61.37 ± 8.73	-
Gender (F: M)	31:13	12:18	-
Age at symptom onset (years)	-	59.10 ± 9.69	-
Disease duration (months)	-	29.20 ± 33.00	-
ALSFRS-R	-	32.67 ± 11.37	-
NfL (pg/mL)	16.39 ± 6.97	112.70 ± 182.20	< 0.005
CXCL10 (pg/mL)	113.60 ± 73.99	304.10 ± 590.20	< 0.05
CCL19 (pg/mL)	106.70 ± 57.37	191.10 ± 175.60	< 0.05
CCL3 (pg/mL)	5.70 ± 2.24	8.47 ± 8.57	< 0.05

Note: Data are presented as mean ± SD unless otherwise indicated. Group comparisons were performed using Welch's *t*-test

Abbreviations: *ALS* amyotrophic lateral sclerosis, *ALSFRS-R* ALS functional rating scale-revised, *HC* healthy control, *NfL* neurofilament light chain

TDP-43 significantly increased the expression of *Cxcl10*, *Ccl3*, and *Ccl19*, an effect significantly attenuated by DHE treatment (Fig. 7B). Consistent with the transcriptional findings, secretion of CXCL10 and CCL3 into ACM was markedly increased by FUS P525L or TDP-43 expression and was significantly reduced by DHE treatment (Fig. 7C). CCL19 protein concentrations could not be reliably quantified because levels in conditioned medium were below the detection limit of the ELISA assay.

Together, these findings identify CXCL10, CCL3, and CCL19 as inflammatory mediators elevated in ALS patient plasma and induced by FUS and TDP-43 expression in astrocytes, with CXCL10 and CCL3 being suppressed by DHE at both the transcriptional and secreted protein levels.

DHE activated NRF2-dependent antioxidant gene expression in astrocytes expressing FUS P525L or TDP-43

To investigate whether DHE engages antioxidant signaling pathways in addition to suppressing NF-κB activation, we examined the expression of genes associated with the NRF2-mediated antioxidant response. Although DHE reportedly activates NRF2 signaling via interacting with KEAP1 in non-neural cell types [3], its effects on NRF2 signaling in astrocytes under ALS/FTD-related proteinopathy conditions remain unknown. The expression of the canonical NRF2 target genes *Cat*, *Nqo1*, and *Hmox1* significantly increased following DHE treatment in both FUS P525L- and TDP-43-expressing astrocytes (Fig. 8A). Similar induction was also observed in control astrocytes treated with DHE. In contrast, overexpression of FUS P525L or TDP-43 alone did not substantially increase expression of these NRF2 target genes.

In contrast, the expression of mitochondrial antioxidant gene *Sod2* was elevated in astrocytes expressing FUS P525L or TDP-43 relative to control cells and was significantly reduced following DHE treatment (Fig. 8B). As *Sod2* induction in stressed mitochondria is widely recognized as a compensatory response to elevated mitochondrial ROS rather than a primary NRF2-driven event [37, 38], and because both FUS and TDP-43 independently increase mitochondrial ROS levels [39, 40], the elevated basal *Sod2* expression observed in FUS P525L- and TDP-43-expressing astrocytes likely reflects an adaptive transcriptional response to the increased oxidative burden associated with these proteinopathies. Within this context, the reduction in *Sod2* expression following DHE treatment is unlikely to indicate suppression of antioxidant defense. Instead, it is more consistent with a reduction in the underlying oxidative stress, thereby diminishing the compensatory requirement for *Sod2* upregulation. Together with the robust induction of canonical NRF2 target genes, this bidirectional transcriptional pattern supports the notion that DHE enhances antioxidant capacity while concurrently alleviating oxidative stress in astrocytes harboring FUS or TDP-43 proteinopathy.

Discussion

In this study, we demonstrate that DHE attenuates astrocyte-mediated neurotoxicity induced by ALS-associated FUS P525L and mitigates neuroinflammatory signaling in astrocytes, as demonstrated in primary mouse cultures and *Drosophila* glial models. Mechanistically, DHE concurrently suppressed NF-κB-dependent inflammatory signaling and activated NRF2-associated antioxidant responses, revealing a dual mechanism of action. Importantly, DHE exerted comparable neuroprotective effects in both FUS and TDP-43 proteinopathy models, suggesting that it targets pathological pathways shared across major ALS/FTD-associated RNA-binding protein disorders. The translational relevance of these findings is supported by two independent observations. First, DHE reversed $NaAsO_2$-induced increases in FUS accumulation and NF-κB activation in fibroblasts derived from a patient with FUS-associated ALS. Second, CXCL10, CCL3, and CCL19—chemokines induced by FUS P525L or TDP-43 expression in primary astrocytes—were significantly elevated in the plasma of patients with sALS. Collectively, these findings support the clinical relevance of the inflammatory pathways identified in our experimental models and highlight DHE as a candidate therapeutic strategy for glia-driven neurotoxicity associated with FUS and TDP-43 proteinopathy.

Our findings demonstrate that DHE effectively suppresses astrocyte-mediated neurotoxicity in both TDP-43 and FUS proteinopathy models, consistent with accumulating evidence indicating that astrocytes play a pivotal role in ALS pathogenesis through non-cell-autonomous mechanisms [41]. The reduction in neuronal toxicity observed following DHE treatment supports

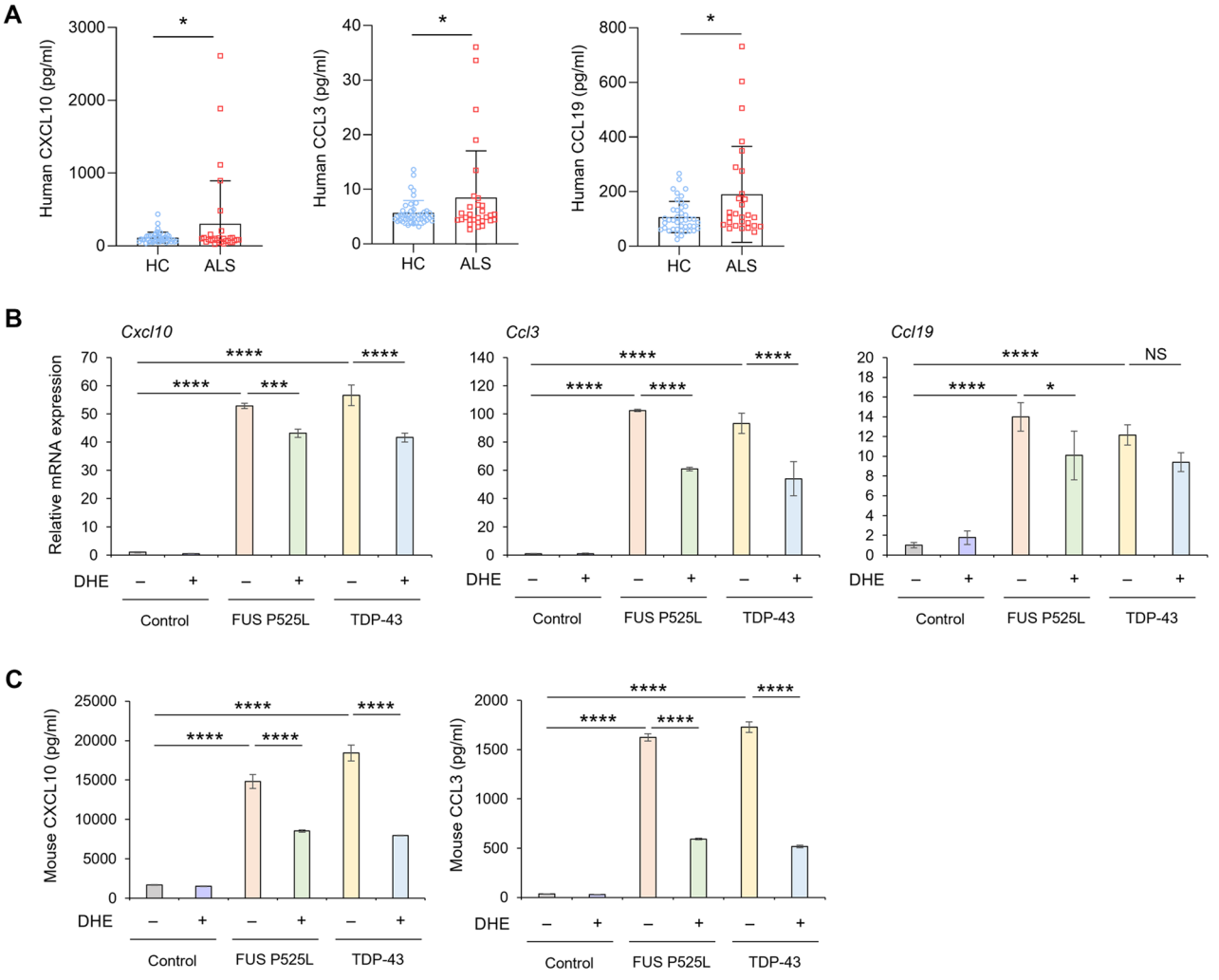

Fig. 7 Inflammatory mediators elevated in ALS plasma are induced by FUS and TDP-43 and suppressed by DHE. **A** Plasma concentrations of CXCL10, CCL3, and CCL19 measured using the Olink Target 48 Cytokine panel in HCs ($n = 44$) and patients with ALS ($n = 30$). Individual data points are shown with mean ± SD. **B** Quantitative RT-qPCR analysis of *Cxcl10*, *Ccl3*, and *Ccl19* expression in primary astrocytes transfected with GFP, FUS P525L, or TDP-43 expression constructs and treated with DHE (10 μM) for 24 h. Gene expression was normalized to *18 S rRNA*. **C** ACM was collected from GFP-, FUS P525L-, or TDP-43-expressing astrocytes following DHE treatment. Secreted CXCL10 and CCL3 protein concentrations were quantified by ELISA. Data are presented as the mean ± SD unless otherwise indicated. Statistical significance was determined using Student's *t*-test (A), or one-way ANOVA followed by Tukey's multiple-comparisons test (B, C). *$p < 0.05$; ***$p < 0.001$; ****$p < 0.0001$; NS, not significant. Cellular experiments were performed independently three times ($n = 3$)

the concept that pharmacological modulation of astrocyte secretory profiles can confer substantial neuroprotection. This interpretation is consistent with recent studies showing that small-molecule interventions can restore neuronal viability in astrocyte-conditioned media assays derived from ALS/FTD-associated mutant models [42]. Given that astrocytes are the key regulators of neuroinflammatory signaling and non-cell-autonomous neuronal injury in ALS/FTD, we focused on astrocyte-mediated pathological mechanisms in the present study. DHE suppressed microglia-mediated neuroinflammation by targeting CYP2A6 in a model of ischemic brain injury [43], indicating that its anti-inflammatory activity extends across multiple glial cell types. Our findings extend these observations by demonstrating a previously unrecognized role for DHE in modulating astrocyte-driven inflammatory responses in ALS/FTD proteinopathy. Although fibroblasts do not directly model CNS inflammation, they provide a clinically relevant validation system in which key molecular effects of DHE are reproduced, further supporting the translational potential of this compound.

The neuroprotective activity of DHE across both FUS and TDP-43 proteinopathy models points to shared pathological mechanisms underlying these RNA-binding protein disorders [15]. Under pathological conditions, both FUS and TDP-43 become mislocalized from the nucleus to the cytoplasm, where they accumulate and

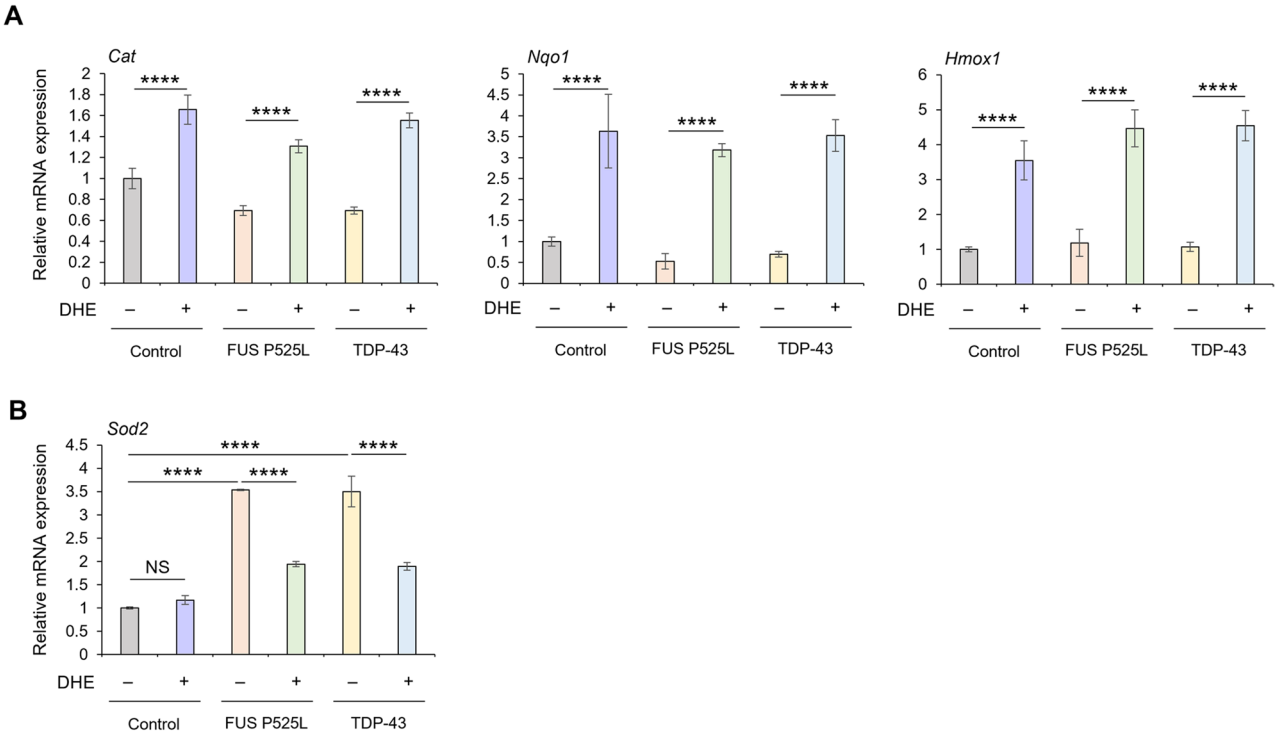

Fig. 8 DHE activates NRF2-associated antioxidant gene expression in astrocytes expressing FUS P525L or TDP-43. **A** Primary astrocytes were transfected with GFP, FUS P525L, or TDP-43 expression constructs and treated with DHE (10 μM) for 24 h. Expression levels of NRF2 target genes *Cat*, *Nqo1*, and *Hmox1* were measured by RT-qPCR and normalized to *18 S rRNA*. **B** Expression of *Sod2* was measured by RT-qPCR in GFP-, FUS P525L-, or TDP-43-expressing astrocytes following DHE treatment and normalized to *18 S rRNA*. Data are presented as mean ± SD from three independent experiments ($n = 3$). Statistical significance was determined using one-way ANOVA followed by Tukey's multiple-comparisons test. ****$p < 0.0001$; NS, not significant

form insoluble aggregates. This disrupts their essential functions in RNA metabolism, including transcriptional regulation, RNA splicing, and mRNA transport [44]. Notably, the aggregation propensity of both proteins is enhanced by oxidative stress, which promotes aberrant phase transitions. Furthermore, recent evidence indicates that TDP-43 aggregation within stress granules is dependent of oxidative stress as a triggering event [45, 46]. The observation that DHE confers protection in both models suggests that it may act on upstream redox-sensitive pathways or downstream effectors shared between FUS- and TDP-43-mediated neurodegeneration.

The elevated plasma concentrations of CXCL10, CCL3, and CCL19 in patients with sALS closely paralleled their increased expression in astrocytes expressing FUS P525L or TDP-43, providing a translational link between our experimental models and human disease. Previous studies have reported elevated levels of CCL3 (MIP-1α) in both cerebrospinal fluid and plasma, as well as increased CXCL10 in the cerebrospinal fluid of patients with ALS [47, 48]. Astrocytes act as major sources of chemokines under pathological conditions, and chemokines such as CXCL10 and CCL3 have been implicated in glial activation and the propagation of neuroinflammatory signaling in neurodegenerative disorders [49]. In addition, cytokine- and chemokine-mediated inflammatory signaling has been linked to neuronal mitochondrial dysfunction and neurotoxicity [50, 51], further supporting the pathological relevance of these mediators in ALS. Notably, elevated CCL19 has not previously been reported in ALS biofluids or large-scale biomarker analyses, suggesting that it may represent a previously unrecognized component of the ALS inflammatory signature that warrants further validation in independent cohorts. CXCL10 has been implicated in the initiation of microglial activation and amplification of neuroinflammatory cascades [52], whereas CCL3 contributes to the formation of neurotoxic glial secretome [53], supporting their potential utility as both biomarkers and candidate therapeutic targets. The suppression of these chemokines by DHE further suggests that modulation of inflammatory signaling contributes to its neuroprotective activity. This observation is particularly relevant in light of growing evidence that neuroinflammation is an active driver of disease progression rather than merely a secondary consequence of neurodegeneration in ALS.

To our knowledge, this is the first study to demonstrate the neuroprotective effects of DHE in ALS/FTD-associated proteinopathy models, although DHE has previously shown therapeutic potential across a broad range of

pathological conditions, including cancer, osteoporosis, inflammatory disorders, and infectious diseases [3, 4, 54–57]. Mechanistically, DHE interacts with multiple stress-responsive signaling pathways that are highly relevant to neurodegeneration. It inhibits NF-κB signaling through interaction with the ATP-binding pocket of IKKα/β, activates NRF2 signaling through covalent modification of KEAP1, suppresses fatty acid synthesis through inhibition of ATP citrate lyase [3, 58], exhibits antidepressant-like activity through high-affinity binding to monoamine oxidase A [8], and modulates PI3K/AKT/mTOR signaling through inhibition of AKT Ser473 phosphorylation [59]. The ability of DHE to simultaneously regulate multiple pathways involved in inflammation, oxidative stress, cellular metabolism, and stress adaptation may contribute to its broad neuroprotective effects observed across both FUS and TDP-43 proteinopathy models.

Beyond its anti-inflammatory activity, we investigated whether DHE provides protection against FUS- and TDP-43-associated pathology. DHE has been characterized as a KEAP1-binding activator of NRF2 signaling in peripheral cell types [3], and NRF2 is widely recognized as a central regulator of redox homeostasis, proteostasis, and cellular stress responses in neurodegenerative disorders [60]. However, whether DHE engages this pathway in astrocytes under proteinopathy-associated stress conditions had not previously been examined. In our study, DHE did not substantially alter the expression of major autophagy- or ubiquitin–proteasome-related genes (data not shown). In contrast, DHE robustly induced the canonical NRF2 target genes *Cat*, *Nqo1*, and *Hmox1* in both FUS- and TDP-43-expressing astrocytes, indicating activation of an NRF2-dependent antioxidant program in CNS cells.

Sod2 exhibited a distinct expression profile. This observation is consistent with the view that *Sod2* induction frequently represents a compensatory response to mitochondrial oxidative stress rather than a direct NRF2-dependent transcriptional response and is often regulated by FOXO3 and other redox-sensitive transcription factors [37, 38]. Both FUS and TDP-43 impair mitochondrial function and increase mitochondrial ROS levels in motor neurons and other cell types [39, 40], providing a plausible explanation for the elevated basal *Sod2* expression observed in our proteinopathy models.

The reduction in *Sod2* expression following DHE treatment is unlikely to reflect suppression of antioxidant defenses. Instead, it is more consistent with a reduction in the underlying oxidative burden, thereby diminishing the compensatory requirement for *Sod2* upregulation.

Together, the induction of canonical NRF2 target genes and normalization of stress-associated *Sod2* expression suggest that DHE enhances antioxidant capacity while alleviating oxidative stress responses in astrocytes expressing pathogenic FUS or TDP-43. Given that oxidative stress promotes aberrant phase transitions and aggregation of RNA-binding proteins [45, 46] and contributes to astrocyte-mediated neurotoxic signaling [40], activation of the NRF2 pathway likely represents an important component of the protective effects of DHE that complements its inhibition of NF-κB-dependent inflammation.

Notably, neuronal mitochondrial function improved following DHE treatment in an ACM paradigm, indicating that this effect is most likely mediated indirectly through alterations in the astrocyte secretome rather than through a direct action on neuronal mitochondria. Chronic inflammatory signaling and oxidative stress are well-established contributors to mitochondrial dysfunction and metabolic impairment in the central nervous system [50, 51, 61]. Therefore, DHE may improve neuronal mitochondrial function through a combined effect of reduced NF-κB-driven inflammatory signaling and enhanced NRF2-associated antioxidant responses. However, mitochondrial ROS was not directly measured in the present study. Consequently, although our findings are consistent with a reduction in oxidative stress, definitive confirmation of this mechanism will require direct redox measurements and genetic or pharmacological loss-of-function studies targeting the NRF2 pathway.

Taken together, the pleiotropic actions of DHE—including suppression of astrocyte-mediated neurotoxicity, attenuation of inflammatory signaling, activation of NRF2-associated antioxidant responses, and protection against mitochondrial dysfunction—suggest that DHE simultaneously modulates multiple pathogenic pathways relevant to ALS and FTD. Such polypharmacological activity may be particularly advantageous for complex neurodegenerative disorders in which multiple interconnected disease mechanisms operate in parallel. Further studies are warranted to define the direct molecular targets of DHE and to optimize its therapeutic potential in neurodegenerative disease.

This study has several limitations. Although DHE improved functional outcomes in *Drosophila* models and exhibited consistent protective effects across mouse and human cellular systems, its efficacy was not evaluated in a mammalian in vivo model of ALS/FTD. Future studies using rodent disease models will be necessary to establish pharmacokinetic properties, optimal dosing regimens, target engagement, and therapeutic efficacy in a mammalian setting. In addition, the patient-derived fibroblast experiments were performed using cells obtained from a single individual carrying a *FUS* mutation; therefore, the clinical relevance of these findings requires validation in a larger cohort of genetically diverse ALS/FTD patient-derived cell lines.

Conclusions

We identified DHE as a promising therapeutic candidate that attenuates astrocyte-mediated neurotoxicity, neuroinflammatory signaling, and mitochondrial dysfunction in models of FUS- and TDP-43-associated proteinopathy. The protective effects of DHE were consistently observed across primary cell cultures, *Drosophila* models, patient-derived fibroblasts, and analyses of ALS patient plasma biomarkers, supporting the translational relevance of the pathways identified in this study. Our findings further suggest that FUS and TDP-43, despite distinct genetic origins, converge on shared pathogenic mechanisms involving astrocyte activation, inflammatory signaling, oxidative stress responses, and non-cell-autonomous neurotoxicity. These results support the concept that therapeutic strategies targeting astrocyte-mediated pathological processes may have broad applicability across ALS/FTD subtypes associated with RNA-binding protein dysfunction.

Abbreviations

ACM	Astrocyte-conditioned medium
AAEB	average enzymes per bead
ALS	Amyotrophic lateral sclerosis
ALSFRS-R	Amyotrophic Lateral Sclerosis Functional Rating Scale–Revised
ANOVA	Analysis of variance
BBB	Blood–brain barrier
CCK-8	Cell Counting Kit-8
CCL	C-C motif chemokine ligand
CNS	Central nervous system
CXCL	C-X-C motif chemokine ligand
DHE	Dehydrocostus lactone
DMEM	Dulbecco's modified Eagle medium
ELISA	Enzyme-linked immunosorbent assay
EtOH	Ethanol
FBS	Fetal bovine serum
FCCP	Carbonyl cyanide 4-(trifluoromethoxy)phenylhydrazone
FTD	Frontotemporal dementia
FUS	Fused in sarcoma
GFP	Green fluorescent protein
HC	Healthy control
HDAC1	Histone deacetylase 1
HMOX1	Heme oxygenase 1
IFN-γ	Interferon gamma
IKK	Inhibitor of nuclear factor kappa-B kinase
IL	Interleukin
IMD	Immune deficiency
iNOS	Inducible nitric oxide synthase
KEAP1	Kelch-like ECH-associated protein 1
LPS	Lipopolysaccharide
$NaAsO_2$	Sodium arsenite
NF-κB	Nuclear factor kappa B
NfL	Neurofilament light chain
NQO1	NAD(P)H quinone dehydrogenase 1
NO	Nitric oxide
Nrf2	Nuclear factor erythroid 2–related factor 2
OCR	Oxygen consumption rate
PBS	Phosphate-buffered saline
PI3K	Phosphoinositide 3-kinase
qRT-PCR	Quantitative reverse transcription polymerase chain reaction
RGP	Resorufin β-D-galactopyranoside
ROS	Reactive oxygen species
sALS	Sporadic amyotrophic lateral sclerosis
SD	Standard deviation
SEM	Standard error of the mean
Simoa	Single-molecule array
SOD2	Superoxide dismutase 2
TDP-43	TAR DNA-binding protein 43
TNF-α	Tumor necrosis factor alpha

Supplementary Information

The online version contains supplementary material available at https://doi.org/10.1186/s12964-026-03082-w.

Supplementary Material 1.

Supplementary Material 2.

Acknowledgements

We sincerely appreciate the participants for their generous donation of samples.

Authors' contributions

M.J., S.K., S.L., S.R.K., M.N. and H.J.K. designed the study and wrote the manuscript. M.J., S.K., J.W., and S.L. performed research. S.H.K., and J-S.P. contributed to clinical sample acquisition and phenotyping. M.J., S.K., and S.L. analyzed data. All authors read and approved of the final manuscript.

Funding

This research was supported by KBRI basic research program through Korea Brain Research Institute funded by Ministry of Science and ICT (26-BR-02-03); and the National Research Foundation of Korea (NRF) grant funded by the Korea government (MSIT) (RS-2024-00343239, RS-2024-00454715).

Data availability

The datasets used and analyzed during the current study are available from the corresponding author upon reasonable request.

Declarations

Ethics approval and consent to participate

This study involving human blood was approved by the institutional review board of the Kyungpook National University Chilgok Hospital, Daegu, South Korea (KNUMC-2023–01-036-001). The Institutional Review Board of Hanyang University Hospital (HYUH 2011-08-010, HYUH 2017-01-043-002) approved the study protocol involving human fibroblast cell. The Animal Care and Use Committee at the animal facility of Korea Brain Research Institute authorized all animal experiments and experimental procedures (IACUC-24-00017).

Consent for publication

Not applicable.

Competing interests

The authors declare no competing interests.

Author details

[1]Dementia Research Group, Korea Brain Research Institute (KBRI), Daegu 41062, Korea, Republic Of
[2]Department of Neurology, School of Medicine, Kyungpook National University, Kyungpook National University Chilgok Hospital, Daegu 41404, Korea, Republic Of
[3]Department of Neurology, College of Medicine, Hanyang University, Seoul 04763, Korea, Republic Of
[4]Cell Therapy Center, Hanyang University Medical Center, Seoul 04763, Korea, Republic Of
[5]School of Life Science and Biotechnology, BK21 FOUR KNU Creative BioResearch Group, Kyungpook National University, Daegu 41566, Korea, Republic Of
[6]Brain Science & Engineering Institute, Kyungpook National University, Daegu 41566, Korea, Republic Of
[7]Graduate School, Daegu Gyeongbuk Institute of Science and Technology (DGIST), Daegu 42988, Korea, Republic Of

Received: 11 December 2025 / Accepted: 12 July 2026
Published online: 15 July 2026

References

1. Wang L, Yang M, Zhang C, Huang F. The protective effects of dehydrocostus lactone against TNF-alpha-induced degeneration of extracellular matrix (ECM) in SW1353 cells. Aging. 2020;12(17):17137–49.
2. Wu YX, Jiang FJ, Liu G, Wang YY, Gao ZQ, Jin SH, et al. Dehydrocostus Lactone Attenuates Methicillin-Resistant Staphylococcus aureus-Induced Inflammation and Acute Lung Injury via Modulating Macrophage Polarization. Int J Mol Sci. 2021;22(18):9754.
3. Yuan Y, Hu Q, Liu L, Xie F, Yang L, Li Y, et al. Dehydrocostus Lactone Suppresses Dextran Sulfate Sodium-Induced Colitis by Targeting the IKKalpha/beta-NF-kappaB and Keap1-Nrf2 Signalling Pathways. Front Pharmacol. 2022;13:817596.
4. Wan M, Dai J, Gan A, Wang J, Lin F, Zhang X, et al. A network pharmacology approach to investigate dehydrocostus lactone inhibits the proliferation and epithelial-mesenchymal transition of human gastric cancer cells via regulating the PI3K/Akt and extracellular signal-regulated kinases/mitogen-activated protein kinase signalling pathways. J Pharm Pharmacol. 2023;75(10):1344–56.
5. Cai H, Yang CH, He XL. [Effect of Dehydrocostus Lactone on Proliferation of K562 Cells and Its Mechanism]. Zhongguo Shi Yan Xue Ye Xue Za Zhi. 2019;27(5):1436–9.
6. Li W, Ma YB, Mao YQ, Lin T. Dehydrocostus lactone suppresses cell growth and induces apoptosis in recombinant human papilloma virus–18 HaCaT cells via the PI3K/Akt signaling pathway. Mol Med Rep. 2018;17(6):7925–30.
7. Wang J, Yu Z, Wang C, Tian X, Huo X, Wang Y, et al. Dehydrocostus lactone, a natural sesquiterpene lactone, suppresses the biological characteristics of glioma, through inhibition of the NF-kappaB/COX-2 signaling pathway by targeting IKKbeta. Am J Cancer Res. 2017;7(6):1270–84.
8. Abebe T, Hymete A, Giday M, Bisrat D. Antidepressant-Like Activity and Molecular Docking Analysis of a Sesquiterpene Lactone Isolated from the Root Bark of Ximenia americana (L). Evid Based Complement Alternat Med. 2024;2024:6680821.
9. Valori CF, Sulmona C, Brambilla L, Rossi D. Astrocytes: Dissecting Their Diverse Roles in Amyotrophic Lateral Sclerosis and Frontotemporal Dementia. Cells-Basel. 2023;12(11):1450.
10. Yang K, Liu Y, Zhang M. The Diverse Roles of Reactive Astrocytes in the Pathogenesis of Amyotrophic Lateral Sclerosis. Brain Sci. 2024;14(2):158.
11. Bustos LM, Sattler R. The Fault in Our Astrocytes - cause or casualties of proteinopathies of ALS/FTD and other neurodegenerative diseases? Front Mol Med. 2023;3:1075805.
12. Canals I, Comella-Bolla A, Cepeda-Prado E, Avaliani N, Crowe JA, Oburoglu L, et al. Astrocyte dysfunction and neuronal network hyperactivity in a CRISPR engineered pluripotent stem cell model of frontotemporal dementia. Brain Commun. 2023;5(3):fcad158.
13. Stoklund Dittlau K, Terrie L, Baatsen P, Kerstens A, De Swert L, Janky R, et al. FUS-ALS hiPSC-derived astrocytes impair human motor units through both gain-of-toxicity and loss-of-support mechanisms. Mol Neurodegener. 2023;18(1):5.
14. Carey JL, Guo L. Liquid-Liquid Phase Separation of TDP-43 and FUS in Physiology and Pathology of Neurodegenerative Diseases. Front Mol Biosci. 2022;9:826719.
15. Mackenzie IR, Rademakers R, Neumann M. TDP-43 and FUS in amyotrophic lateral sclerosis and frontotemporal dementia. Lancet Neurol. 2010;9(10):995–1007.
16. de Boer EMJ, Orie VK, Williams T, Baker MR, De Oliveira HM, Polvikoski T, et al. TDP-43 proteinopathies: a new wave of neurodegenerative diseases. J Neurol Neurosurg Psychiatry. 2020;92(1):86–95.
17. Smethurst P, Risse E, Tyzack GE, Mitchell JS, Taha DM, Chen YR, et al. Distinct responses of neurons and astrocytes to TDP-43 proteinopathy in amyotrophic lateral sclerosis. Brain. 2020;143(2):430–40.
18. Peng AYT, Agrawal I, Ho WY, Yen YC, Pinter AJ, Liu J, et al. Loss of TDP-43 in astrocytes leads to motor deficits by triggering A1-like reactive phenotype and triglial dysfunction. Proc Natl Acad Sci U S A. 2020;117(46):29101–12.
19. Wu S, Yin Y, Du L. FUS aggregation following ischemic stroke favors brain astrocyte activation through inducing excessive autophagy. Exp Neurol. 2022;355:114144.
20. Ajmone-Cat MA, Onori A, Toselli C, Stronati E, Morlando M, Bozzoni I, et al. Increased FUS levels in astrocytes leads to astrocyte and microglia activation and neuronal death. Sci Rep. 2019;9(1):4572.
21. Kia A, McAvoy K, Krishnamurthy K, Trotti D, Pasinelli P. Astrocytes expressing ALS-linked mutant FUS induce motor neuron death through release of tumor necrosis factor-alpha. Glia. 2018;66(5):1016–33.
22. Enokido Y, Akaneya Y, Niinobe M, Mikoshiba K, Hatanaka H. Basic fibroblast growth factor rescues CNS neurons from cell death caused by high oxygen atmosphere in culture. Brain Res. 1992;599(2):261–71.
23. Araki W, Yuasa K, Takeda S, Shirotani K, Takahashi K, Tabira T. Overexpression of presenilin-2 enhances apoptotic death of cultured cortical neurons. Ann N Y Acad Sci. 2000;920:241–4.
24. McCarthy KD, de Vellis J. Preparation of separate astroglial and oligodendroglial cell cultures from rat cerebral tissue. J Cell Biol. 1980;85(3):890–902.
25. Livak KJ, Schmittgen TD. Analysis of relative gene expression data using real-time quantitative PCR and the 2(-Delta Delta C(T)) Method. Methods. 2001;25(4):402–8.
26. Dranka BP, Benavides GA, Diers AR, Giordano S, Zelickson BR, Reily C, et al. Assessing bioenergetic function in response to oxidative stress by metabolic profiling. Free Radic Biol Med. 2011;51(9):1621–35.
27. Lim SM, Choi WJ, Oh KW, Xue Y, Choi JY, Kim SH, et al. Directly converted patient-specific induced neurons mirror the neuropathology of FUS with disrupted nuclear localization in amyotrophic lateral sclerosis. Mol Neurodegener. 2016;11:8.
28. Kim HJ, Raphael AR, LaDow ES, McGurk L, Weber RA, Trojanowski JQ, et al. Therapeutic modulation of eIF2alpha phosphorylation rescues TDP-43 toxicity in amyotrophic lateral sclerosis disease models. Nat Genet. 2014;46(2):152–60.
29. Pandey UB, Nie Z, Batlevi Y, McCray BA, Ritson GP, Nedelsky NB, et al. HDAC6 rescues neurodegeneration and provides an essential link between autophagy and the UPS. Nature. 2007;447(7146):859–63.
30. Feany MB, Bender WW. A Drosophila model of Parkinson's disease. Nature. 2000;404(6776):394–8.
31. Hua X, Wang Y, Yang C, Chai R, Li X, Tayier G, et al. Effect of incubation with lipopolysaccharide and interferon-gamma on reactive astrogliosis. J Integr Neurosci. 2019;18(4):415–21.
32. Zhou B, Wang H, Cai Y, Wen H, Wang L, Zhu M, et al. FUS P525L mutation causing amyotrophic lateral sclerosis and movement disorders. Brain Behav. 2020;10(6):e01625.
33. Yih LH, Peck K, Lee TC. Changes in gene expression profiles of human fibroblasts in response to sodium arsenite treatment. Carcinogenesis. 2002;23(5):867–76.
34. Wang L, Shi W, Gao X, SreeHarsha N, Zhang D. Cardioprotective role of metformin against sodium arsenite-induced oxidative stress, inflammation, and apoptosis. IUBMB Life. 2020;72(4):749–57.
35. Al-Megrin WA, Metwally DM, Habotta OA, Amin HK, Abdel Moneim AE, El-Khadragy M. Nephroprotective effects of chlorogenic acid against sodium arsenite-induced oxidative stress, inflammation, and apoptosis. J Sci Food Agric. 2020;100(14):5162–70.
36. Lee S, Kim S, Kang HY, Lim HR, Kwon Y, Jo M, et al. The overexpression of TDP-43 in astrocytes causes neurodegeneration via a PTP1B-mediated inflammatory response. J Neuroinflammation. 2020;17(1):299.
37. Flynn JM, Melov S. SOD2 in mitochondrial dysfunction and neurodegeneration. Free Radic Biol Med. 2013;62:4–12.
38. Hagenbuchner J, Ausserlechner MJ. Mitochondria and FOXO3: breath or die. Front Physiol. 2013;4:147.
39. Wang P, Deng J, Dong J, Liu J, Bigio EH, Mesulam M, et al. TDP-43 induces mitochondrial damage and activates the mitochondrial unfolded protein response. PLoS Genet. 2019;15(5):e1007947.
40. Cunha-Oliveira T, Montezinho L, Mendes C, Firuzi O, Saso L, Oliveira PJ, et al. Oxidative Stress in Amyotrophic Lateral Sclerosis: Pathophysiology and Opportunities for Pharmacological Intervention. Oxid Med Cell Longev. 2020;2020:5021694.
41. Rossi S, Cozzolino M. Dysfunction of RNA/RNA-Binding Proteins in ALS Astrocytes and Microglia. Cells. 2021;10(11):3005.
42. Masegosa VM, Fritz E, Corvalan D, Rojas F, Garces P, Navarro X, et al. Novel Dual Mechanism GRT-X Agonist Acting on Kv7 Potassium Channel/Translocator Protein Receptor Prevents Motoneuron Degeneration Following Exposure to Mouse and Human Amyotrophic Lateral Sclerosis/Frontotemporal Dementia Astrocyte-Conditioned Media. ACS Chem Neurosci. 2025;16(15):2887–900.
43. Shu X, Zou X, Zhang J, Fang X, Wang X, Wu H, et al. Dehydrocostus Lactone Inhibits Microglia-Mediated Neuroinflammation by Targeting CYP2A6 to Improve Ischemic Brain Injury. CNS Neurosci Ther. 2025;31(7):e70502.
44. Rummens J, Da Cruz S. RNA-binding proteins in ALS and FTD: from pathogenic mechanisms to therapeutic insights. Mol Neurodegener. 2025;20(1):64.
45. Yan X, Kuster D, Mohanty P, Nijssen J, Pombo-Garcia K, Garcia Morato J, et al. Intra-condensate demixing of TDP-43 inside stress granules generates pathological aggregates. Cell. 2025;188(15):4123–e41404118.

46. Harley J, Clarke BE, Patani R. The Interplay of RNA Binding Proteins, Oxidative Stress and Mitochondrial Dysfunction in ALS. Antioxid (Basel). 2021;10(4):552.
47. Yang X, Gao L, Wu X, Zhang Y, Zang D. Increased levels of MIP-1alpha in CSF and serum of ALS. Acta Neurol Scand. 2016;134(2):94–100.
48. Tateishi T, Yamasaki R, Tanaka M, Matsushita T, Kikuchi H, Isobe N, et al. CSF chemokine alterations related to the clinical course of amyotrophic lateral sclerosis. J Neuroimmunol. 2010;222(1–2):76–81.
49. Kumari S, Dhapola R, Sharma P, Paidlewar M, Vellingiri B, Medhi B, et al. Unravelling neuronal death mechanisms: The role of cytokines and chemokines in immune imbalance in Alzheimer's disease progression. Ageing Res Rev. 2025;112:102883.
50. Dong H, Zhang H, Cai L, Ye Q, Wang H, Liu B, et al. Inflammatory Signaling Induces Mitochondrial Dysfunction and Neuronal Death in Traumatic Brain Injury via Downregulation of OXPHOS Genes. Biochem Genet. 2025;63(6):5394–414.
51. Kuhn MK, Fleeman RM, Beidler LM, Snyder AM, Chan DC, Proctor EA. Amyloid-beta Pathology-Specific Cytokine Secretion Suppresses Neuronal Mitochondrial Metabolism. Cell Mol Bioeng. 2023;16(4):405–21.
52. Trageser KJ, Yang EJ, Smith C, Iban-Arias R, Oguchi T, Sebastian-Valverde M, et al. Inflammasome-Mediated Neuronal-Microglial Crosstalk: a Therapeutic Substrate for the Familial C9orf72 Variant of Frontotemporal Dementia/Amyotrophic Lateral Sclerosis. Mol Neurobiol. 2023;60(7):4004–16.
53. Mai YD, Zhang Q, Fung CL, Leung SO, Chong CH. CD22 modulation alleviates amyloid beta-induced neuroinflammation. J Neuroinflammation. 2025;22(1):32.
54. Endalew SA, Taddese MG, Muhammed M. Evaluation of antioxidant and antibacterial properties of dehydrocostus lactone isolated from Echinops kebericho root. Health Sci Rep. 2024;7(3):e1990.
55. Zhang R, Hao J, Wu Q, Guo K, Wang C, Zhang WK, et al. Dehydrocostus lactone inhibits cell proliferation and induces apoptosis by PI3K/Akt/Bad and ERS signalling pathway in human laryngeal carcinoma. J Cell Mol Med. 2020;24(11):6028–42.
56. Hu B, Wu F, Shi Z, He B, Zhao X, Wu H, et al. Dehydrocostus lactone attenuates osteoclastogenesis and osteoclast-induced bone loss by modulating NF-kappaB signalling pathway. J Cell Mol Med. 2019;23(8):5762–70.
57. Park EJ, Park SW, Kim HJ, Kwak JH, Lee DU, Chang KC. Dehydrocostuslactone inhibits LPS-induced inflammation by p38MAPK-dependent induction of hemeoxygenase-1 in vitro and improves survival of mice in CLP-induced sepsis in vivo. Int Immunopharmacol. 2014;22(2):332–40.
58. Chen Y, Shen J, Yuan M, Li H, Li Y, Zheng S, et al. Dehydrocostus lactone suppresses gastric cancer progression by targeting ACLY to inhibit fatty acid synthesis and autophagic flux. J Adv Res. 2025;67:331–48.
59. Wang CY, Tsai AC, Peng CY, Chang YL, Lee KH, Teng CM, et al. Dehydrocostuslactone suppresses angiogenesis in vitro and in vivo through inhibition of Akt/GSK-3beta and mTOR signaling pathways. PLoS ONE. 2012;7(2):e31195.
60. Zhang DD. Thirty years of NRF2: advances and therapeutic challenges. Nat Rev Drug Discov. 2025;24(6):421–44.
61. Sterling JK, Kam TI, Guttha S, Park H, Baumann B, Mehrabani-Tabari AA, et al. Interleukin-6 triggers toxic neuronal iron sequestration in response to pathological alpha-synuclein. Cell Rep. 2022;38(7):110358.

Publisher's note

Springer Nature remains neutral with regard to jurisdictional claims in published maps and institutional affiliations.